Cell Stem Cell
Article

Autocrine TGF-β Signaling Maintains Tumorigenicity of Glioma-Initiating Cells through Sry-Related HMG-Box Factors

Hiroaki Ikushima,[1] Tomoki Todo,[2,3] Yasushi Ino,[2,3] Masamichi Takahashi,[2] Keiji Miyazawa,[1] and Kohei Miyazono[1,*]
[1]Department of Molecular Pathology
[2]Department of Neurosurgery
[3]Translational Research Center
Graduate School of Medicine, University of Tokyo, Tokyo 113-0033, Japan
*Correspondence: miyazono@m.u-tokyo.ac.jp
DOI 10.1016/j.stem.2009.08.018

SUMMARY

Despite aggressive surgery, radiotherapy, and chemotherapy, treatment of malignant glioma remains formidable. Although the concept of cancer stem cells reveals a new framework of cancer therapeutic strategies against malignant glioma, it remains unclear how glioma stem cells could be eradicated. Here, we demonstrate that autocrine TGF-β signaling plays an essential role in retention of stemness of glioma-initiating cells (GICs) and describe the underlying mechanism for it. TGF-β induced expression of Sox2, a stemness gene, and this induction was mediated by Sox4, a direct TGF-β target gene. Inhibitors of TGF-β signaling drastically deprived tumorigenicity of GICs by promoting their differentiation, and these effects were attenuated in GICs transduced with Sox2 or Sox4. Furthermore, GICs pretreated with TGF-β signaling inhibitor exhibited less lethal potency in intracranial transplantation assay. These results identify an essential pathway for GICs, the TGF-β-Sox4-Sox2 pathway, whose disruption would be a therapeutic strategy against gliomas.

INTRODUCTION

Glioblastoma multiforme (GBM), the most malignant form of glioma, is one of the most aggressive human cancers with a 5 year survival rate of less than one out of ten (Surawicz et al., 1998). Despite past huge efforts, this statistic has not markedly improved over the past years. Excessive proliferation, diffuse infiltration into surrounding brain tissue, and suppression of antitumor immune surveillance contribute to the malignant phenotype of glioblastomas.

Cancer-initiating cells (cancer stem cells, CSCs) are rare tumor cells characterized by their ability to induce tumorigenesis and to self-renew. Recent concepts for cancer suggest that a minority population of CSCs may determine the biological and pathological characters of tumors. Similar to other tumors, glioma-initiating cells (glioma stem cells, GSCs) have been isolated from human glioma tissues and several glioma cell lines (Singh et al., 2004; Kondo et al., 2004; Hirschmann-Jax et al., 2004). GSCs are characterized by the expression of neural stem cell (NSC) antigens and the ability to grow as nonadherent spheres termed "neurospheres" or "glioma spheres" when cultured in the presence of epidermal growth factor (EGF) and basic fibroblast growth factor (bFGF) under serum-free condition. Thus, GSCs share several characteristics with normal NSCs (Vescovi et al., 2006).

According to the concept of CSCs, failure to cure cancer may be attributed to the current therapeutic strategies, which have been aimed at the tumor bulk without significantly affecting CSCs. Like other CSCs, GSCs have been reported to be resistant to conventional radiation and pharmacological therapies (Bao et al., 2006; Liu et al., 2006a). Although elimination of CSCs has been regarded as a prerequisite for the development of successful therapeutic strategies, it has not still been fully elucidated how their stemness is maintained. To establish therapeutic strategies against glioma, in vitro and in vivo models that faithfully recapitulate the stem cell component of gliomas have been developed. Among these models, glioma spheres cultured in serum-free media supplemented with EGF and bFGF are considered to reflect biological and pathological characters of primary glioma tissues, have ability to self-renew, and mimic original tumors after intracranial transplantation (Singh et al., 2004; Lee et al., 2006).

Although transforming growth factor (TGF)-β suppresses proliferation of certain carcinoma cells and is well known to be a tumor suppressor, it promotes proliferation of tumors of nonepithelial origin, including glioma and osteosarcoma, through induction of PDGF-BB (Bruna et al., 2007; Matsuyama et al., 2003). TGF-β binds to type I and type II serine/threonine kinase receptors and transduces intracellular signals principally through Smad proteins (Derynck and Zhang, 2003; Massagué, 2008; Miyazawa et al., 2002). Upon phosphorylation by type I receptors, receptor-regulated Smads (R-Smads; Smad2 and -3) form heteromeric complexes with common-partner Smad (Co-Smad; Smad4), translocate into the nucleus, and regulate expression of various target genes. In addition to induction of proliferation, TGF-β pathway has also been implicated in invasion, metastasis, and intratumoral angiogenesis of glioma. These multiple roles of TGF-β in glioma progression have promoted the development of therapeutic agents based on the inhibition of the TGF-β pathway (Golestaneh and Mishra, 2005).

Here, we report that autocrine TGF-β signaling induces Sox2 expression, one of the crucial factors for maintenance of NSCs,

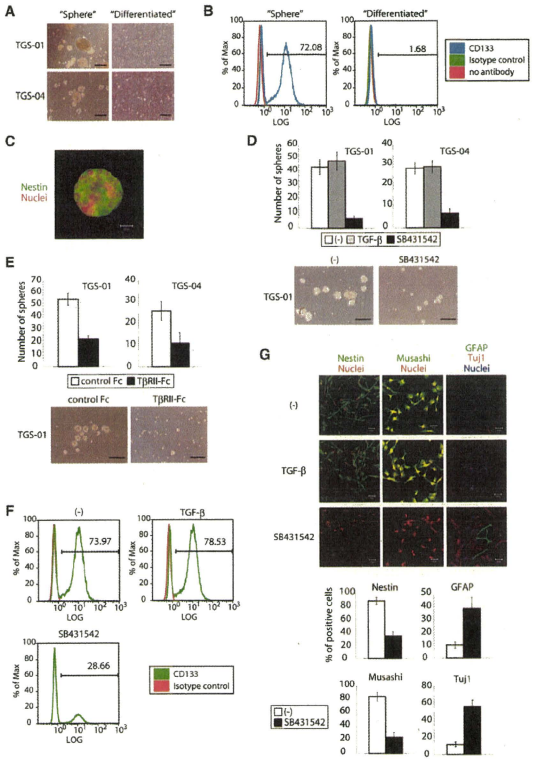

Figure 1. TGF-β Signaling Maintains Stemness of Glioma-Initiating Cells

(A) Representative images of glioma spheres TGS-01 and TGS-04 cultured in serum-free neurobasal media with EGF and bFGF ("Sphere"), and glioma cells derived from the same pathological samples as spheres but cultured in media containing 10% fetal bovine serum ("Differentiated"). Scale bars, 100 μm.

(B) CD133$^+$ ratio of "Sphere" cells (TGS-01) and "Differentiated" cells was determined by flow cytometry.

(C) TGS-01 spheres were stained with Nestin. Scale bars, 20 μm.

(D) TGF-β inhibitor deprives glioma-initiating cells of sphere-forming ability. Glioma-initiating cells were dissociated into single-cell populations and cultured with TGF-β ligand (100 pM) or inhibitor (SB431542, 1 μM) for 7 days. The data are presented as the number of glioma spheres formed (means ± SEM of five fields). Scale bars, 100 μm.

(E) Glioma-initiating cells were dissociated into single-cell populations and cultured with human TGF-β RII/Fc chimera (1 μg/ml) or control IgG_1 Fc (1 μg/ml) for 7 days. The data are presented as the number of glioma spheres formed (means ± SEM of five fields). Scale bars, 100 μm.

(F) Effects of TGF-β ligand (100 pM) or inhibitor (SB431542, 1 μM) on CD133$^+$ subpopulation of TGS-01 cells were determined by flow cytometry.

(G) Immunostaining of TGS-01 cells. Spheres were disaggregated, seeded on poly-L-ornithine and fibronectin-coated slide glasses, and cultured in serum-free medium with TGF-β ligand (100 pM) or inhibitor (SB431542, 1 μM) for 7 days. Quantification of Nestin-, Musashi-, Tuj1-, or GFAP-positive cells was shown in the bottom graphs. Scale bars, 50 μm.

and plays essential roles in maintenance of stemness of the glioma-initiating cells. We also demonstrate that another Sry-related high-mobility group (HMG) box-containing gene, Sox4, is a crucial mediator of TGF-β-induced Sox2 expression. Notably, glioma-initiating cells pretreated with TGF-β signaling inhibitor were less aggressive and showed less lethal potency in intracranial transplantation assay. These findings open the way to depriving GSCs of the tumorigenic activity and will offer new therapeutic possibilities.

RESULTS

Inhibition of TGF-β Signaling Deprives Glioma-Initiating Cells of Tumorigenic Activity

To study the mechanisms of how stemness of glioma-initiating cells is maintained, we have used glioma tissues obtained from two patients with GBM. They were cultured in serum-free medium and termed TGS-01 and TGS-04 (Figure 1A), both of which have the ability to self-renew and mimic the original tumor after transplantation into the brains of immunocompromised mice (Lee et al., 2006). Profiles of the patients and properties of the GBM cells are described in Figure S1 (in Supplemental Data available online). Expression of phosphatase and tensin homolog (Pten) was lost in TGS-01 and TGS-04 "sphere" cells. CD133 (Prominin-1) was reported to be a marker for GSCs (Singh et al., 2004). We confirmed that the CD133$^+$ subpopulation is enriched in these glioma spheres compared to cells derived from the same patient but cultured in media containing 10% fetal bovine serum ("Differentiated" or "Adherent") (Sphere; 72.0%, Differentiated; 1.6%, Figure 1B). In addition, tumor spheres derived from each of tissue samples could be passaged serially and expressed Nestin (neural precursor cell marker), confirming that these are clonogenic and self-renewing cells (Figure 1C). We also validated enrichment of glioma-initiating cells in TGS-01 and TGS-04 "sphere" cells by an intracranial transplantation assay (M.T., Y.I., and T.T., unpublished data).

To test a possible role of TGF-β signaling in glioma-initiating cells, we first examined the effect of inhibition of TGF-β signaling

on their biological characters. After treatment with TGF-β type I receptor (ALK5) kinase inhibitor SB431542 (Inman et al., 2002), glioma-initiating cells were drastically deprived of sphere-forming ability (Figure 1D). Similar results were obtained using three other glioma-initiating cells from patients with GBM (Figures S1 and S2). As SB431542 can inhibit TGF-β type I receptor (ALK5) signaling, as well as activin/nodal type I receptor (ALK4 and ALK7) signaling, we also examined the effect of TGF-β receptor II/Fc chimera (TβRII-Fc) on glioma-initiating cells to assess the role of TGF-β signaling definitely. Glioma-initiating cells treated with TβRII-Fc formed glioma spheres with lower efficiency (Figure 1E). Similar results were obtained with other TGF-β signaling inhibitors, A-78-03 (Tojo et al., 2005) or LY364947 (Sawyer et al., 2003) (Figure S3A), as well as infection of adenovirus carrying cDNA of Smad7, an endogenous negative regulator of TGF-β signaling (Figure S3B). Moreover, preformed sphere cells lost their spherical growth pattern and became attached in the presence of SB431542 (Figure S3C). Decreased number of glioma spheres formed by glioma-initiating cells with depleted TGF-β signaling suggests impaired self-renewal. In agreement with the suggested effect of TGF-β signaling depletion, treatment of glioma-initiating cells with SB431542 for 7 days prior to the sphere-forming assay without the inhibitor also reduced the number of spheres (Figure S4). We also investigated the effects of TGF-β inhibitor on the $CD133^+$ subpopulation. SB431542 decreased the size of $CD133^+$ pool in glioma-initiating cells (Figure 1F). Next, to examine the expression of neural precursor or differentiation markers in each cell, spheres in serum-free medium were disaggregated and seeded on poly-L-ornithine and fibronectin-coated slide glasses. Inhibition of TGF-β signaling decreased the number of cells positive for Nestin or Musashi (neural precursor cell markers) and increased that for GFAP (astrocyte differentiated marker) or Tuj1 (βIII-tubulin, neuronal marker) (Figure 1G). Taken together, these findings suggest endogenous TGF-β signaling maintains tumorigenicity and stemness of glioma-initiating cells. Conversely, we failed to observe striking effects of addition of TGF-β ligand on sphere-forming ability, $CD133^+$ ratio, or marker expression of glioma-initiating cells (Figures 1D, 1F, and 1G). It may be because glioma-initiating cells express all the major components of TGF-β signaling pathway and secrete TGF-β1 and -β2 proteins (Figures S5A and S5B), producing sufficient autocrine TGF-β signaling to maintain their stemness (Figure S5C).

TGF-β is reported to work as a proapoptotic or an antiapoptotic factor in a cell-context-dependent manner (Sánchez-Capelo, 2005; Ehata et al., 2007), but we failed to observe any significant effect of TGF-β ligand or inhibitor on apoptosis of glioma-initiating cells (Figure S6A). TGF-β is also known to control cell proliferation via regulating $p15^{INK4B}$, $p21^{WAF1}$, $p27^{KIP1}$, and *c-myc* (Massagué, 2008), but in glioma-initiating cells, stimulation or inhibition of TGF-β signaling did not markedly affect their expression levels at 3 or 24 hr except for only a slight increase of $p21^{WAF1}$ 24 hr after inhibition of TGF-β signaling (Figure S6B).

Sox2 Expression Is Induced by TGF-β in Glioma-Initiating Cells to Maintain Their Stemness

To elucidate the mechanism by which stemness of glioma-initiating cells is maintained by TGF-β signaling, we next examined the effect of TGF-β or SB431542 on expression of various markers for stemness. mRNA expression of Sox2, a member of HMG-box factors, was induced by TGF-β but suppressed by SB431542 after 24 hr treatment (Figure 2A) and kept at the low levels for at least 7 days (data not shown). In contrast, expression levels of Oct4, Nanog, LIF, or other pluripotent stem cell-related molecules were not significantly affected by TGF-β ligand or inhibitor in our glioma-initiating cells in TGS-01 and -04 cells (Figure S7), although Nanog and LIF were reported to be induced by TGF-β stimulation in some types of cells (Xu et al., 2008; Bruna et al., 2007). Induction of Sox2 by TGF-β was clearly suppressed in the presence of siRNA against Smad2 and Smad3 (Figure 2B), indicating that Sox2 expression is regulated by TGF-β-Smad signaling. We also confirmed regulation of Sox2 protein expression by TGF-β and SB431542 (Figure 2C). Knockdown of Sox2 expression by siRNA (Figure S8) resulted in drastic reduction of sphere-forming ability and self-renewal capacity of glioma-initiating cells (Figures 2D and 2E) and decreased size of $CD133^+$ subpopulation (75.1% to 29.3% or 35.9%; Figure 2F). Drastic reduction of sphere-forming ability by knockdown of Sox2 was also observed in four other glioma cells (Figure S9). Moreover, the number of Nestin-positive cells was reduced and that of GFAP-positive cells was increased by Sox2 knockdown (Figure 2G). These findings indicate that Sox2 is an essential factor for maintenance of stemness of glioma-initiating cells and that downregulation of Sox2 expression as early as 24 hr after treatment with SB431542 appears to be the cause, rather than the result, of deprivation of stemness of glioma-initiating cells.

Downregulation of Sox2 Is a Crucial Step for Differentiation of Glioma-Initiating Cells Induced by TGF-β Inhibitor

For further study of the role of Sox2 in maintenance of stemness by TGF-β, we examined the effect of TGF-β inhibitor on glioma-initiating cells infected with adenovirus encoding Sox2 cDNA. SB431542 only weakly deprived Sox2-overexpressed glioma-initiating cells of sphere-forming ability compared to LacZ-overexpressed cells (Figure 3A). Moreover, SB431542 failed to reduce the number of Nestin-positive cells or to increase the number of GFAP-positive cells in Sox2-overexpressed glioma-initiating cells (Figure 3B). These data suggest that deprivation of stemness of glioma-initiating cells by TGF-β inhibitor is due to downregulation of Sox2, which maintains stemness of glioma-initiating cells.

Sox4 Is a TGF-β Target Gene, which Is Highly Expressed in Glioma-Initiating Cells

Induction of Sox2 expression by TGF-β was observed 24 hr, but not 3 hr, after stimulation (Figure 2A) and attenuated in the presence of cycloheximide, an inhibitor of protein synthesis (Figure 4A). These findings indicate that Sox2 expression is not directly induced by TGF-β but regulated through other factor(s) that are induced by TGF-β. We, thus, searched candidate genes that mediate TGF-β-induced Sox2 expression to play important roles in retention of stemness of glioma-initiating cells. For this purpose, we used microarray data of public resources (Beier et al., 2007; Bruna et al., 2007; Günther et al., 2008; Lee et al., 2006; Tso et al., 2006). Criteria for selection were as follows: (1) genes with higher expression in glioma-initiating cells compared

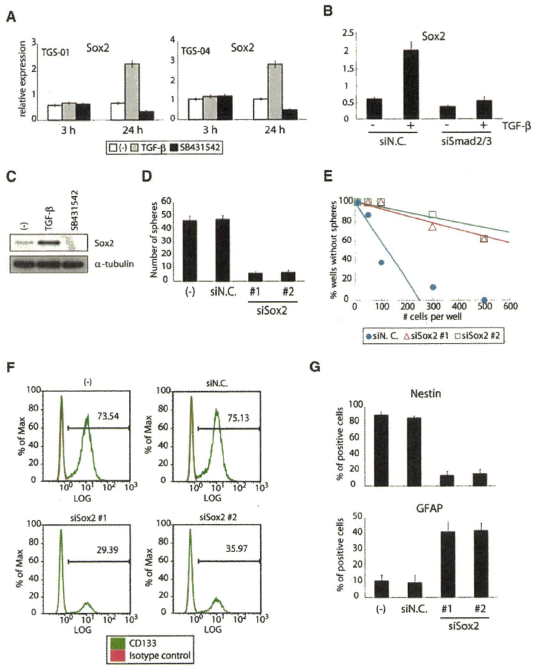

Figure 2. TGF-β Induces Expression of Sox2, an Essential Factor for Retention of Stemness of Glioma-Initiating Cells

(A) Expression of Sox2 mRNA was determined after treatment with TGF-β ligand (100 pM) or inhibitor (SB431542, 1 μM) for 3 or 24 hr. Values were normalized to that of GAPDH mRNA. Error bars represent SEM.

(B) TGS-01 cells were transfected with siRNA oligonucleotides and incubated for 24 hr. Cells were treated with TGF-β ligand (100 pM) for 24 hr. Values were normalized to that of GAPDH mRNA. Error bars represent SEM.

(C) Expression of Sox2 protein in TGS-01 cells was determined after treatment with TGF-β ligand (100 pM) or inhibitor (SB431542, 1 μM) for 24 hr. α-tubulin was used as a loading control.

(D) TGS-01 cells were dissociated into single-cell populations, transfected with control (N.C.) or Sox2 siRNA duplex, and cultured for 7 days. The data are presented as the number of glioma spheres formed (means ± SEM of five fields).

(E) Knockdown of Sox2 expression by siRNA in TGS-01 cells resulted in decrease of self-renewal capacity in limiting dilution assay.

(F) Effects of Sox2 knockdown on CD133$^+$ subpopulation of TGS-01 cells were determined by flow cytometry.

(G) Quantification of Nestin-positive or GFAP-positive cells among total cells. Differentiation of TGS-01 cells by Sox2 knockdown was analyzed 7 days after transfection of control (N.C.) or Sox2 siRNA duplex. Error bars represent SEM.

to bulk tumor cells; (2) genes directly induced by TGF-β and suppressed by TGF-β inhibitor in glioma cells; and (3) genes whose expression levels are correlated with that of Sox2 in glioma cells. Among genes highly expressed in glioma-initiating cells, we identified a transcription factor Sox4 as a TGF-β target gene.

We observed higher expression levels of Sox4 in TGS-01 and TGS-04 cells than in matched "differentiated" cells (Figure 4B). We checked whether Sox4 expression is regulated by TGF-β signaling (Figures 4C and 4D). Sox4 mRNA expression was immediately induced after TGF-β stimulation and inversely downregulated by TGF-β inhibitor in TGS-01 and TGS-04 cells. To examine whether Sox4 is a direct target gene of TGF-β, we performed chromatin immunoprecipitation assay using antibody against Smad2/3, DNA-binding mediators of TGF-β signaling. Smad complexes directly bound to Sox4 promoter in response to TGF-β stimulation, and this binding was clearly suppressed by SB431542 (Figure 4E). Moreover, induction of Sox4 by TGF-β was not significantly affected by cycloheximide (Figure 4F). These findings indicate that Sox4 is a direct target gene of TGF-β signaling.

Sox4 Associates with the Sox2 Enhancer Region and Promotes Its Expression

Next, we studied the effect of Sox4 on Sox2 expression. Sox4 overexpression in glioma-initiating cells resulted in upregulation of Sox2 expression (Figure 5A). In contrast, Sox2 expression was suppressed by Sox4 knockdown (Figure 5B). We confirmed that Sox2 mRNA expressed under the control of cytomegalovirus (CMV) promoter was not downregulated by siSox4 (Figure S10), indicating that Sox2 mRNA is not a direct target of siSox4. These results indicate that Sox2 expression is positively regulated by Sox4 at the transcriptional level. To examine whether this regulation is direct, we performed chromatin immunoprecipitation assay using antibody against Sox4. It has been demonstrated that the enhancer element located at the 3′ flanking region of Sox2 gene is important for regulation of Sox2 expression (Chew et al., 2005; Tomioka et al., 2002). The region contains the consensus binding motif for Sox4, "CATTGTA" (Liao et al., 2008). Recruitment of Sox4 to the enhancer element was increased 24 hr after TGF-β stimulation, and such recruitment was clearly suppressed by SB431542 treatment (Figure 5C). These results appear to be due to regulation of Sox4 expression by TGF-β ligand or inhibitor. In addition, TGF-β could induce Sox2 expression only weakly under the condition that Sox4 was knocked down (Figure 5D). Altogether, we concluded that Sox4 directly induced by TGF-β

upregulates Sox2 expression through association with its enhancer region.

Sox4 Is An Essential Factor for Maintenance of Stemness of Glioma-Initiating Cells

So far, Sox4 has not been reported to have any role in maintenance of stem cell properties. To study the role of Sox4 in glioma-initiating cells, we examined the effect of Sox4 knockdown on stemness of glioma-initiating cells. Sox4-knocked-down glioma-initiating cells showed less sphere-forming ability and self-renewal capacity (Figures 6A and 6B), and the size of $CD133^+$ pool was decreased (72.6% to 41.5% or 41.1%; Figure 6C). Moreover, the number of Nestin-positive cells was decreased, while that of GFAP-positive cells was increased by Sox4 knockdown (Figure 6D). These results indicate that Sox4 is involved in a crucial pathway for maintenance of stemness of glioma-initiating cells.

Sox4 Plays an Essential Role in Maintenance of Stemness of Glioma-Initiating Cells by TGF-β

From these results, we hypothesized that Sox4 expression directly induced by TGF-β promotes Sox2 expression and maintains stemness of glioma-initiating cells. To test this hypothesis, first, we examined the effect of TGF-β inhibitor on glioma-initiating cells infected with adenovirus carrying cDNA of Sox4. Sox4-overexpressing glioma-initiating cells showed resistance against deprivation of sphere-forming ability by SB431542 (Figure 7A). Moreover, the number of Nestin-positive cells and that of GFAP-positive cells of Sox4-overexpressed glioma-initiating cells were minimally affected by SB431542 (Figure 7B). These data suggest that direct induction of Sox4 expression by TGF-β plays essential roles in maintenance of stemness of glioma-initiating cells.

TGF-β Inhibitor Deprives Glioma-Initiating Cells of In Vivo Tumorigenic Activity through Downregulation of Sox4 Expression

To study the role of TGF-β-induced Sox4 in maintenance of stemness in vivo, we examined the effects of TGF-β inhibitor and Sox4 on intracranial growth of glioma-initiating cells (Figure 7C). As TGF-β is well known to promote proliferation of bulk glioma cells, SB431542 was used in pretreatment, rather than successive treatment, to distinguish the effect on differentiation from that on proliferation. The survival of the mice inoculated with SB431542-pretreated glioma-initiating cells was significantly prolonged compared to mice injected with control glioma-initiating cells. All mice bearing control glioma-initiating cells developed neurological signs and displayed large tumors. In contrast, all mice bearing SB431542-pretreated glioma-initiating cells did not develop neurological signs and the brains showed no evidence of tumor by pathological examination with H&E staining. Furthermore, the survival advantage effect of SB431542 was not observed for Sox4-transduced glioma-initiating cells (Figure 7C). Altogether, we concluded that TGF-β upregulates Sox2 expression through direct induction of Sox4 to sustain stemness of glioma-initiating cells and that TGF-β inhibitor blocks this pathway to deprive them of aggressiveness (Figure 7D).

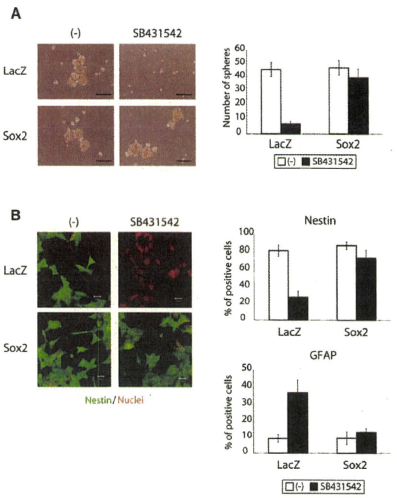

Figure 3. Downregulation of Sox2 Expression by TGF-β Inhibitor Is a Critical Step for Differentiation of Glioma-Initiating Cells

(A) Representative images of TGS-01 cells infected with adenovirus-Sox2 or LacZ (negative control) and cultured with or without SB431542 (1 μM) for 7 days. The data are presented as the number of glioma spheres formed (means ± SEM of five fields). Scale bars, 100 μm.

(B) Marker expression of TGS-01 cells infected with adenovirus-Sox2 or LacZ and cultured with or without SB431542 (1 μM) for 7 days. Images of Nestin-positive cells are shown in the left panels. Quantification of Nestin-positive or GFAP-positive cells among total cells is shown in the right graphs. Error bars represent SEM. Scale bars, 20 μm.

DISCUSSION

TGF-β was reported to induce epithelial-mesenchymal transition (EMT) in immortalized human mammary epithelial cells and increase the ability to form mammospheres (Mani et al., 2008). These findings suggest a direct link between EMT and the gain of epithelial stem cell properties of carcinoma. Such a link could be applied to other carcinoma stem cells than breast CSCs. However, since glioma cells per se have nonepithelial characters, the link may not be applied to GSCs.

To analyze roles of TGF-β signaling in glioma stem cells, we have used glioma tissues obtained from patients with GBM and they were cultured in serum-free medium ("sphere"). All of the ten mice injected intracranially with 5×10^3 TGS-01 "sphere" cells were killed within 70 days after transplantation, while all of the ten mice bearing 5×10^5 matched "differentiated" cells had survived for more than 140 days without neurological signs (M.T., Y.I., and T.T., unpublished data). These results indicate that populations with a higher tumorigenic activity were enriched in "sphere" cells.

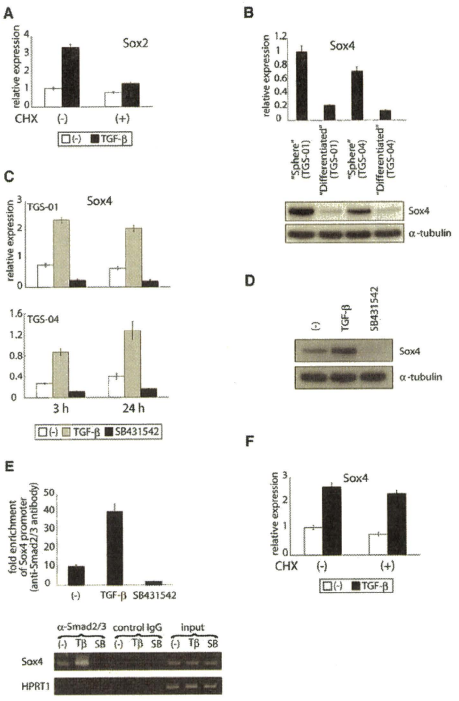

Figure 4. Sox4 Is a Direct Target Gene of TGF-β Signaling

(A) Expression levels of Sox2 mRNA after TGF-β (100 pM) treatment for 24 hr. Treatment with cycloheximide (CHX, 3 μg/ml) was started 30 min before stimulation with TGF-β. Values were normalized to amounts of GAPDH mRNA. Error bars represent SEM.

(B) Expression levels of Sox4 mRNA and protein in "Sphere" cells and "Differentiated" cells. α-tubulin was used as a loading control.

(C) Amount of Sox4 mRNA was determined after TGF-β ligand (100 pM) or inhibitor (SB431542, 1 μM) treatment for 3 or 24 hr. Values were normalized to that of GAPDH mRNA. Error bars represent SEM.

(D) Amount of Sox4 protein was determined after TGF-β ligand (100 pM) or inhibitor (SB431542, 1 μM) treatment for 24 hr. α-tubulin was used as a loading control.

(E) Association of Smad complex with the Sox4 promoter. Chromatin immunoprecipitation analysis was performed using TGS-01 cells treated with TGF-β ligand (100 pM) or inhibitor (SB431542, 1 μM) for 1.5 hr. Eluted DNAs were subjected to quantitative real-time PCR analysis (graph) or conventional RT-PCR (figure). In real-time PCR analysis, values were normalized to the amount of the first intron of hypoxanthine phosphoribosyltransferase (HPRT) 1. Error bars represent SEM. Input, 1%.

(F) Expression levels of Sox4 were analyzed using cDNAs, which were prepared in the experiments shown in (A).

We have shown here that inhibition of TGF-β signaling induces differentiation of glioma-initiating cells and that TGF-β maintains stemness of these cells through induction of Sox2 expression. Moreover, we have demonstrated that Sox4 is a direct target of TGF-β and that Sox4 mediates TGF-β-induced Sox2 expression. Although inhibition of TGF-β signaling markedly promoted differentiation of glioma-initiating cells, addition of TGF-β ligand failed to induce substantial change in glioma-initiating cells. It may be because TGF-β ligand is sufficiently produced by glioma-initiating cells for maintenance of their stemness at the basal level (Figure S5) in spite of the findings that TGF-β signaling itself is not saturated (Figures 2A, 2C, 4C, and 4D). Consistent with these results, overexpression of Sox4 or Sox2 in glioma-initiating cells did not affect their sphere-forming ability in the presence of autocrine TGF-β signaling. These results indicate that in glioma-initiating cells Sox4 and Sox2 are present at sufficient levels for retention of their aggressiveness in the presence of autocrine TGF-β signaling.

Bone morphogenetic protein (BMP) 4, another member of the TGF-β family, promotes differentiation and depletes the pool of glioma-initiating cells (Piccirillo et al., 2006). BMP signaling is known to control the activity of normal brain stem cells (Lim et al., 2000), and TGF-β signaling also regulates normal brain development (Golestaneh and Mishra, 2005; Muñoz-Sanjuán and Brivanlou, 2002). Altogether, the roles of TGF-β and BMP signaling in GSCs may reflect those in normal NSCs, supporting the concept that GSCs and NSCs are closely related (Vescovi et al., 2006).

Sox2 is well known to be one of the self-renewal genes, such as Oct4 and Nanog, and to play pivotal roles in maintaining stemness of embryonic stem cells (Kamachi et al., 2000). Sox2 null mutant embryos cannot give rise to embryonic or trophectoderm lineages (Gubbay et al., 1990). Introduction of Sox2 together with Oct4, Klf4, and c-Myc to human or mouse adult fibroblasts results in generation of induced pluripotent stem (iPS) cells (Takahashi and Yamanaka, 2006; Takahashi et al., 2007). Sox2 also plays essential roles in maintenance of NSCs (Graham et al., 2003), and Sox2 deficiency causes impaired neurogenesis in adult mouse brain (Ferri et al., 2004). Although it was reported that glioma tissues highly express Sox2 mRNA compared to nonmalignant tissues (Ben-Porath et al., 2008; Schmitz et al., 2007), the role of Sox2 in the development of glioma has not yet been determined. In glioma cells, expression levels of Sox2 are linearly and exponentially correlated with those of Nestin and CD133, respectively (Figure S11A, data set from Lee et al., 2006). Here, we demonstrated that knockdown of Sox2 resulted in deprivation of tumorigenic activity of glioma-initiating cells. Our report is the first to show significance of Sox2 in development of glioma and maintenance of the aggressive characters of glioma cells. The results that Sox2 is an essential factor for

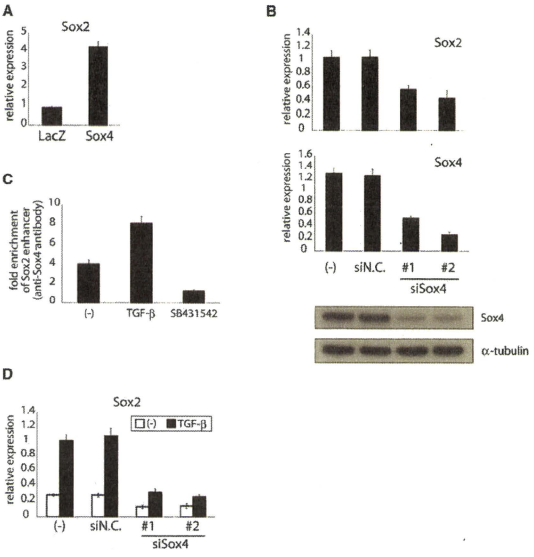

Figure 5. Sox4 Is a Crucial Mediator for TGF-β-Induced Sox2 Expression

(A) Effects of Sox4 overexpression on expression of Sox2. TGS-01 cells were infected with adenovirus-Sox4 or LacZ 24 hr before harvest. Values were normalized to the amount of GAPDH mRNA. Error bars represent SEM.

(B) Effects of Sox4 knockdown on expression of Sox2. Upper graphs show mRNA levels of Sox2 and Sox4. RNA levels were normalized to amounts of GAPDH mRNA. Error bars represent SEM. Lower panels show protein levels of Sox4 and α-tubulin.

(C) Association of Sox4 with the Sox2 enhancer. Chromatin immunoprecipitation analysis was performed using TGS-01 cells treated with TGF-β ligand (100 pM) or inhibitor (SB431542, 1 μM) for 24 hr. Eluted DNAs were subjected to quantitative real-time PCR analysis. Values were normalized to the amount of the first intron of HPRT1. Error bars represent SEM.

(D) TGF-β-induced Sox2 expression under the condition of Sox4 knockdown. Expression levels of Sox2 mRNA after TGF-β (100 pM) treatment for 24 hr were determined by real-time PCR. Indicated siRNAs were transfected 24 hr before TGF-β treatment.

maintenance of GSCs as well as NSCs and embryonic stem cells support the concept that malignant cancer cells and normal developing cells are closely associated with each other in their biological properties. Because Sox2 is a crucial factor for maintenance of other tissue stem cells, it can be speculated that Sox2 also plays significant roles in maintenance of other CSCs.

Although Sox2 is already known to play crucial roles to maintain stemness of NSCs, Sox4 has not been reported to have any function in stem cell properties. So far, Sox4 was reported to be overexpressed in glioma tissues compared to normal brain tissues (Tso et al., 2006), but its role in the development of glioma has not been determined. Here, we have demonstrated that Sox4 binds to Sox2 enhancer region and plays important roles in sustaining tumorigenicity of glioma-initiating cells. From the public data sets, we found that glioma-initiating cells show higher expression of Sox2 and Sox4 and that their expression levels significantly correlate with each other (Figures S11B and S11C, data set from Lee et al., 2006), suggesting that the TGF-β-Sox4-Sox2 pathway is widely used in glioma-initiating cells for retention of their stemness. These findings may add a new player, Sox4, to the concept of stemness.

Sox4 contains a DNA-binding domain known as the HMG box and has been shown to be a transcriptional activator involved in the development of the cardiac outflow tract and the central nervous system (Cheung et al., 2000). So far, Sox4 overexpression has been found to be associated with several human cancer types, including not only glioma but also hepatic cellular carcinoma, prostate cancer, lung cancer, bladder carcinoma, and medulloblastoma (Aaboe et al., 2006; Lee et al., 2002; Liao et al., 2008; Liu et al., 2006b; Pramoonjago et al., 2006; Yokota et al., 2004). The mechanism of Sox4 function as an oncogene, however, has not been fully investigated. From our report, Sox4 can be defined as an oncogene with new mechanisms, at least in glioblastoma.

Although we demonstrated that the TGF-β-Sox4-Sox2 pathway is indispensable for the maintenance of stemness of glioma-initiating cells, the possibility cannot be excluded that other signaling pathways are also involved in it. Hedgehog signaling has been implicated in the development of glioma for many years. It was reported that Hedgehog-Gli1 pathway regulates the stemness of glioma-initiating cells and that cyclopamine, a hedgehog inhibitor, could reduce glioma tumor volume (Clement et al., 2007), though the mechanisms by which inhibition of Hedgehog-Gli1 pathway promotes differentiation of glioma-initiating cells were not investigated. Cyclopamine abrogated sphere-forming ability of TGS-01 cells, but this effect was weaker than that of SB431542, and these two agents failed to show additive or synergistic effects (Figure S12). Therefore, it is likely that there are at least two types of GSCs, Hedgehog-Gli1 pathway-dependent cells and TGF-β-Sox4-Sox2 pathway-dependent cells. To apply Hedgehog inhibitor and TGF-β inhibitor to clinical stages, it will be necessary to assess GSCs of each patient for their signal dependency.

While this manuscript was under revision, Peñuelas et al. (2009) independently reported that TGF-β increases glioma-initiating cell self-renewal through induction of LIF in human glioblastoma. Their results agree with our report in terms of the role

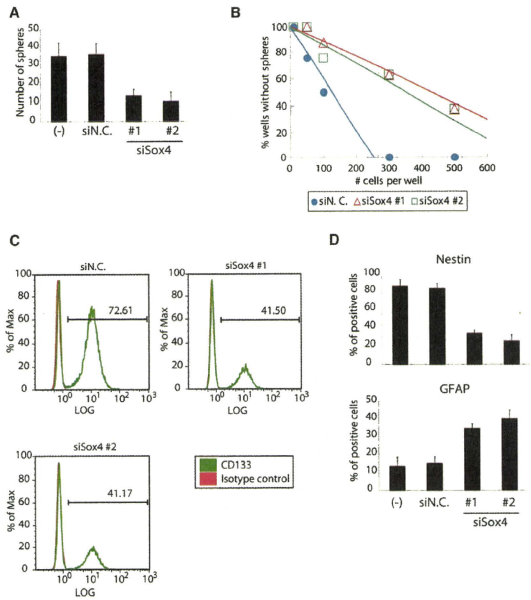

Figure 6. Sox4 Plays Important Roles in Maintenance of Stemness of Glioma-Initiating Cells

(A) TGS-01 cells were dissociated into single-cell populations, transfected with control or Sox4 siRNA duplex, and cultured for 7 days. The data are presented as the number of glioma spheres formed (means ± SEM of five fields).

(B) Knockdown of Sox4 expression by siRNA in TGS-01 cells resulted in a decrease of self-renewal capacity in limiting dilution assay.

(C) Effects of Sox4 knockdown on $CD133^+$ subpopulation of TGS-01 cells were determined by flow cytometry.

(D) Quantification of Nestin-positive or GFAP-positive cells among total cells. Differentiation of TGS-01 cells by Sox4 knockdown was analyzed 7 days after transfection of control (N.C.) or Sox4 siRNA duplex. Error bars represent SEM.

of TGF-β signaling in maintenance of glioma-initiating cells. Although glioma-initiating cells used in our study, TGS-01 and -04, were deprived of their tumorigenicity in the presence of anti-LIF neutralizing antibody (Figure S13), TGF-β signaling failed to induce LIF expression (Figure S7). Taken together, TGF-β signaling may maintain tumorigenicity of glioma-initiating cells through multiple (at least two) independent pathways.

To target TGF-β signaling in glioma, clinical studies of a TGF-β2-specific antisense oligonucleotide AP 12009 in recurrent or refractory high-grade glioma are ongoing (Schlingensiepen et al., 2006). Our findings indicate that such TGF-β inhibitors should be delivered to GSCs, not only to the tumor bulk. This indication will thus pursue the realization of new therapeutic strategies, inducing differentiation of GSCs in addition to suppressing bulk tumor growth. Classical pharmacological therapies cannot sufficiently eradicate GSCs (Liu et al., 2006a). Moreover, GSCs were known to be resistant against radiotherapy (Bao et al., 2006). Our results raise the possibility that TGF-β inhibitors can be used in a combination therapy with classical pharmacological therapies and radiation to make glioblastoma less aggressive. To achieve this, we need to develop a method for delivery of TGF-β inhibitor to GSCs. Delivery of TGF-β inhibitor to GSCs without affecting the functions of normal brain tissues may improve prognosis of GBM, one of the most lethal malignant tumors.

EXPERIMENTAL PROCEDURES

Cell Culture and Reagents

Primary grade IV glioblastoma samples were obtained during surgery from consenting patients, as approved by the Institutional Review Board at the University of Tokyo Hospital (Characteristics of the patients are listed in Figure S1A). Spheres were cultured in DMEM/F12 serum-free medium (Invitrogen) supplemented with B27 (Invitrogen), 20 ng/ml of EGF, and 20 ng/ml of bFGF (both from PeproTech). The antibodies used were as follows: anti-Musashi (Chemicon), anti-Nestin (Chemicon), anti-GFAP (Dako), anti-Tuj1 (Covance), anti-Sox2 (R&D), anti-Sox4 (Santa Cruz), anti-α-tubulin (Sigma-Aldrich), anti-phospho-Smad2 (Zymed Laboratories), anti-Smad2/3 (BD Transduction Laboratories), and phycoerythrin-conjugated CD133/2 (293C3) antibody (Miltenyi Biotec). SB431542 and cycloheximide were purchased from Sigma-Aldrich. Recombinant human TGF-β RII/Fc chimera was from R&D Systems.

Immunostaining

Glioma-initiating cells were seeded on poly-L-ornithine (Sigma)- and fibronectin (Sigma)-coated slide glasses and cultured for 7 days with indicated ligands or inhibitors in serum-free medium. Cells were fixed with 3.7% paraformaldehyde, permealized with PBS containing 0.3% Triton X-100, and incubated with indicated antibodies. Subsequently, samples were incubated with secondary antibodies and stained with propidium iodide (Molecular Probes) for nuclear staining. Stained cells were observed with a confocal microscope (LSM510, Carl Zeiss).

Flow Cytometry

Cells were dissociated into single-cell populations and labeled with a phycoerythrin-conjugated CD133 antibody. The expression level was analyzed using a Beckman Coulter EPICS XL flow cytometer with EXPO32 ADC software.

Sphere-Forming Assay

Glioma-initiating cells were cultured in non-tissue-culture-treated flask (BD Biosciences) with vented caps (BD Biosciences) for 7 days. Floated spheres in five fields per each sample were counted under a microscope (magnification, ×40).

RNA Interference

Small interfering RNAs (siRNAs, see Table S1 for sequences) were purchased from Invitrogen and introduced into cells using Oligofectamine transfection reagent (Invitrogen) according to the manufacturer's instructions.

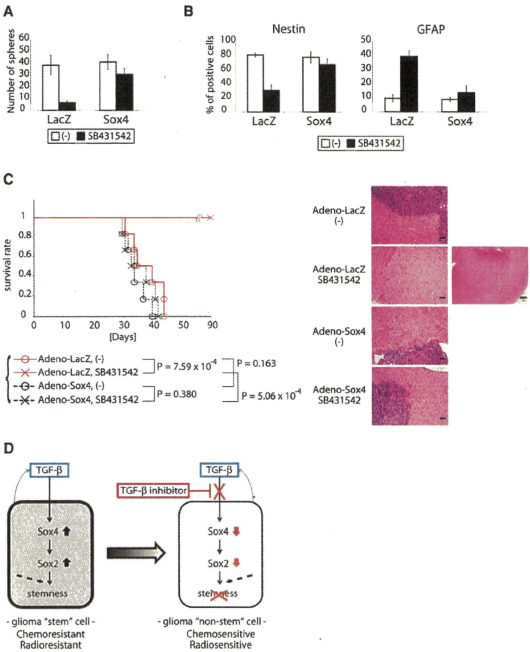

Figure 7. Direct Suppression of Sox4 Expression by TGF-β Inhibitor Is a Critical Step for Differentiation of Glioma-Initiating Cells In Vitro and In Vivo

(A) TGS-01 cells were dissociated into single-cell populations, infected with adenovirus-Sox4 or LacZ, and cultured with or without SB431542 (1 μM) for 7 days. The data are presented as the number of glioma spheres formed (means ± SEM of five fields).

(B) Marker expression of TGS-01 cells infected with adenovirus-Sox4 or LacZ and cultured with or without SB431542 (1 μM) for 7 days. Quantification of Nestin-positive or GFAP-positive cells among total cells is shown in graphs. Error bars represent SEM.

(C) Development of gliomas after intracranial transplantation of 5 × 10^4 TGS-01 cells infected with adenovirus-Sox4 or LacZ (negative control) and treated with or without TGF-β inhibitor (SB431542, 1 μM) for 24 hr. Survival of mice (n = 6 mice for each condition) was evaluated by Kaplan-Meier analysis (left graph). p value was calculated using a log-rank test. Right panels show the results of histological examination of the samples dissected at 30 days after intracranial transplantation. Tissue sections were stained with hematoxylin and eosin. Scale bars, 50 μm in the four left images (×20) or 300 μm in the right image (×4).

(D) Model of maintenance of stemness of glioma-initiating cells by autocrine TGF-β signaling. TGF-β directly induces Sox4 expression. Subsequently, Sox4 promotes expression of Sox2, which plays significant roles in sustaining stemness of glioma-initiating cells, possibly in cooperation with other signaling pathways (dotted arrows). TGF-β inhibitor blocks this "TGF-β-Sox4-Sox2" pathway, promotes differentiation of glioma-initiating cells, and deprives them of aggressiveness.

Adenoviruses

Flag-tagged full-length Sox2 and Sox4 cDNAs were cloned into a pENTR vector (Invitrogen) and introduced into the adenoviral genome via recombination between pENTR vector and the pAd/CMV/V5-DEST vector using LR Clonase (Invitrogen). HEK293A cells were infected with pAd/CMV/Sox2 or pAd/CMV/Sox4 after linearization of it with *PacI*. Viral particles were isolated by three freeze-thaw cycles and amplified by reinfection to HEK293A cells.

Cell Lysis and Immunoblotting

Cells were lysed with a buffer containing 1% Nonidet P-40, 20 mM Tris-HCl (pH 7.4), 150 mM NaCl, 1 mM PMSF, 1% aprotinin, and 5 mM EDTA. Proteins in cleared cell lysates were subjected to SDS-PAGE and transferred to Fluoro Trans W membrane (Pall). Immunoblotting was performed using the indicated antibodies.

Quantitative Real-Time PCR

Quantitative real-time reverse transcription PCR was performed as described previously (Ikushima et al., 2008). All samples were run in triplicate in each experiment. The primers used are listed in Table S1. Values were normalized to that for glyceraldehyde-3-phosphate dehydrogenase (GAPDH).

Limiting Dilution Assay

Sphere cells were dissociated and plated in 96-well plates in 200 μl serum-free medium. After a 7 day culture, the percentage of wells not containing spheres for each cell-plating density was calculated and plotted against the number of cells per well.

Chromatin Immunoprecipitation

Chromatin immunoprecipitation was performed as described previously (Koinuma et al., 2009). Following reverse crosslinking, DNA was treated with proteinase K and purified using a PCR purification kit (QIAGEN). DNA was eluted in 30 μl of TE and used for PCR analysis or quantitative real-time PCR. PCR primers are listed in Table S1.

Intracranial Proliferation Assay

Viable glioma-initiating cells (5 × 10^4) in 5 μl of DMEM/F12 medium were injected stereotactically into the right cerebral hemisphere of 5-week-old female BALB/c *nu/nu* mice at a depth of 3 mm. All animal experimental protocols were performed in accordance with the policies of the Animal Ethics Committee of the University of Tokyo.

Statistical Analysis of Microarray Data

Microarray data were obtained from GEO (http://www.ncbi.nlm.nih.gov/geo/) and ArrayExpress (http://www.ebi.ac.uk/microarray/). Data were analyzed with statistical software R (http://www.R-project.org).

SUPPLEMENTAL DATA

Supplemental Data include one table and 13 figures and can be found with this article online at http://www.cell.com/cell-stem-cell/supplemental/S1934-5909(09)00402-0.

ACKNOWLEDGMENTS

We are grateful to Yasuyuki Morishita, Daisuke Itoh, Hiroshi Yoshida, and Chihana Fujita for skilled technical assistance. This work was supported by KAKENHI (Grant-in-aid for Scientific Research) and Global COE Program (Integrative Life Science Based on the Study of Biosignaling Mechanisms) from the Ministry of Education, Culture, Sports, Science, and Technology of Japan. H.I. has been supported by a Tetsumon-scholarship for the Ph.D.-M.D. program of the University of Tokyo and by a research fellowship of the Japan Society for the Promotion of Science for Young Scientists.

Received: March 12, 2009
Revised: June 17, 2009
Accepted: August 10, 2009
Published: November 5, 2009

REFERENCES

Aaboe, M., Birkenkamp-Demtroder, K., Wiuf, C., Sørensen, F.B., Thykjaer, T., Sauter, G., Jensen, K.M., Dyrskjøt, L., and Ørntoft, T. (2006). SOX4 expression in bladder carcinoma: clinical aspects and in vitro functional characterization. Cancer Res. *66*, 3434–3442.

Bao, S., Wu, Q., McLendon, R.E., Hao, Y., Shi, Q., Hjelmeland, A.B., Dewhirst, M.W., Bigner, D.D., and Rich, J.N. (2006). Glioma stem cells promote radioresistance by preferential activation of the DNA damage response. Nature *444*, 756–760.

Beier, D., Hau, P., Proescholdt, M., Lohmeier, A., Wischhusen, J., Oefner, P.J., Aigner, L., Brawanski, A., Bogdahn, U., and Beier, C.P. (2007). CD133(+) and CD133(-) glioblastoma-derived cancer stem cells show differential growth characteristics and molecular profiles. Cancer Res. *67*, 4010–4015.

Ben-Porath, I., Thomson, M.W., Carey, V.J., Ge, R., Bell, G.W., Regev, A., and Weinberg, R.A. (2008). An embryonic stem cell-like gene expression signature in poorly differentiated aggressive human tumors. Nat. Genet. *40*, 499–507.

Bruna, A., Darken, R.S., Rojo, F., Ocaña, A., Peñuelas, S., Arias, A., Paris, R., Tortosa, A., Mora, J., Baselga, J., et al. (2007). High TGFbeta-Smad activity confers poor prognosis in glioma patients and promotes cell proliferation depending on the methylation of the PDGF-B gene. Cancer Cell *11*, 147–160.

Cheung, M., Abu-Elmagd, M., Clevers, H., and Scotting, P.J. (2000). Roles of Sox4 in central nervous system development. Brain Res. Mol. Brain Res. *79*, 180–191.

Chew, J.L., Loh, Y.H., Zhang, W., Chen, X., Tam, W.L., Yeap, L.S., Li, P., Ang, Y.S., Lim, B., Robson, P., et al. (2005). Reciprocal transcriptional regulation of Pou5f1 and Sox2 via the Oct4/Sox2 complex in embryonic stem cells. Mol. Cell. Biol. *25*, 6031–6046.

Clement, V., Sanchez, P., de Tribolet, N., Radovanovic, I., and Ruiz i Altaba, A. (2007). HEDGEHOG-GLI1 signaling regulates human glioma growth, cancer stem cell self-renewal, and tumorigenicity. Curr. Biol. *17*, 165–172.

Derynck, R., and Zhang, Y.E. (2003). Smad-dependent and Smad-independent pathways in TGF-beta family signalling. Nature *425*, 577–584.

Ehata, S., Hanyu, A., Hayashi, M., Aburatani, H., Kato, Y., Fujime, M., Saitoh, M., Miyazawa, K., Imamura, T., and Miyazono, K. (2007). Transforming growth factor-beta promotes survival of mammary carcinoma cells through induction of antiapoptotic transcription factor DEC1. Cancer Res. *67*, 9694–9703.

Ferri, A.L., Cavallaro, M., Braida, D., Di Cristofano, A., Canta, A., Vezzani, A., Ottolenghi, S., Pandolfi, P.P., Sala, M., DeBiasi, S., et al. (2004). Sox2 deficiency causes neurodegeneration and impaired neurogenesis in the adult mouse brain. Development *131*, 3805–3819.

Golestaneh, N., and Mishra, B. (2005). TGF-beta, neuronal stem cells and glioblastoma. Oncogene *24*, 5722–5730.

Graham, V., Khudyakov, J., Ellis, P., and Pevny, L. (2003). SOX2 functions to maintain neural progenitor identity. Neuron *39*, 749–765.

Gubbay, J., Collignon, J., Koopman, P., Capel, B., Economou, A., Münsterberg, A., Vivian, N., Goodfellow, P., and Lovell-Badge, R. (1990). A gene mapping to the sex-determining region of the mouse Y chromosome is a member of a novel family of embryonically expressed genes. Nature *346*, 245–250.

Günther, H.S., Schmidt, N.O., Phillips, H.S., Kemming, D., Kharbanda, S., Soriano, R., Modrusan, Z., Meissner, H., Westphal, M., and Lamszus, K. (2008). Glioblastoma-derived stem cell-enriched cultures form distinct subgroups according to molecular and phenotypic criteria. Oncogene *27*, 2897–2909.

Hirschmann-Jax, C., Foster, A.E., Wulf, G.G., Nuchtern, J.G., Jax, T.W., Gobel, U., Goodell, M.A., and Brenner, M.K. (2004). A distinct "side population" of cells with high drug efflux capacity in human tumor cells. Proc. Natl. Acad. Sci. USA *101*, 14228–14233.

Ikushima, H., Komuro, A., Isogaya, K., Shinozaki, M., Hellman, U., Miyazawa, K., and Miyazono, K. (2008). An Id-like molecule, HHM, is a synexpression group-restricted regulator of TGF-β signalling. EMBO J. *27*, 2955–2965.

Inman, G.J., Nicolás, F.J., Callahan, J.F., Harling, J.D., Gaster, L.M., Reith, A.D., Laping, N.J., and Hill, C.S. (2002). SB-431542 is a potent and specific inhibitor of transforming growth factor-beta superfamily type I activin receptor-like kinase (ALK) receptors ALK4, ALK5, and ALK7. Mol. Pharmacol. *62*, 65–74.

Kamachi, Y., Uchikawa, M., and Kondoh, H. (2000). Pairing SOX off: with partners in the regulation of embryonic development. Trends Genet. *16*, 182–187.

Koinuma, D., Tsutsumi, S., Kamimura, N., Taniguchi, H., Miyazawa, K., Sunamura, M., Imamura, T., Miyazono, K., and Aburatani, H. (2009). Chromatin immunoprecipitation on microarray analysis of Smad2/3 binding sites reveals roles of ETS1 and TFAP2A in transforming growth factor beta signaling. Mol. Cell. Biol. *29*, 172–186. Published online October 27, 2008. 10.1128/MCB.01038-08.

Kondo, T., Setoguchi, T., and Taga, T. (2004). Persistence of a small subpopulation of cancer stem-like cells in the C6 glioma cell line. Proc. Natl. Acad. Sci. USA *101*, 781–786.

Lee, C.J., Appleby, V.J., Orme, A.T., Chan, W.I., and Scotting, P.J. (2002). Differential expression of SOX4 and SOX11 in medulloblastoma. J. Neurooncol. *57*, 201–214.

Lee, J., Kotliarova, S., Kotliarov, Y., Li, A., Su, Q., Donin, N.M., Pastorino, S., Purow, B.W., Christopher, N., Zhang, W., et al. (2006). Tumor stem cells derived from glioblastomas cultured in bFGF and EGF more closely mirror the phenotype and genotype of primary tumors than do serum-cultured cell lines. Cancer Cell *9*, 391–403.

Liao, Y.L., Sun, Y.M., Chau, G.Y., Chau, Y.P., Lai, T.C., Wang, J.L., Horng, J.T., Hsiao, M., and Tsou, A.P. (2008). Identification of SOX4 target genes using phylogenetic footprinting-based prediction from expression microarrays suggests that overexpression of SOX4 potentiates metastasis in hepatocellular carcinoma. Oncogene *27*, 5578–5589.

Lim, D.A., Tramontin, A.D., Trevejo, J.M., Herrera, D.G., García-Verdugo, J.M., and Alvarez-Buylla, A. (2000). Noggin antagonizes BMP signaling to create a niche for adult neurogenesis. Neuron *28*, 713–726.

Liu, G., Yuan, X., Zeng, Z., Tunici, P., Ng, H., Abdulkadir, I.R., Lu, L., Irvin, D., Black, K.L., and Yu, J.S. (2006a). Analysis of gene expression and chemoresistance of CD133+ cancer stem cells in glioblastoma. Mol. Cancer *5*, 67.

Liu, P., Ramachandran, S., Ali Seyed, M., Scharer, C.D., Laycock, N., Dalton, W.B., Williams, H., Karanam, S., Datta, M.W., Jaye, D.L., et al. (2006b). Sex-determining region Y box 4 is a transforming oncogene in human prostate cancer cells. Cancer Res. *66*, 4011–4019.

Mani, S.A., Guo, W., Liao, M.J., Eaton, E.N., Ayyanan, A., Zhou, A.Y., Brooks, M., Reinhard, F., Zhang, C.C., Shipitsin, M., et al. (2008). The epithelial-mesenchymal transition generates cells with properties of stem cells. Cell *133*, 704–715.

Massagué, J. (2008). TGFbeta in cancer. Cell *134*, 215–230.

Matsuyama, S., Iwadate, M., Kondo, M., Saitoh, M., Hanyu, A., Shimizu, K., Aburatani, H., Mishima, H.K., Imamura, T., Miyazono, K., et al. (2003). SB-431542 and

Gleevec inhibit transforming growth factor-beta-induced proliferation of human osteosarcoma cells. Cancer Res. *63*, 7791–7798.

Miyazawa, K., Shinozaki, M., Hara, T., Furuya, T., and Miyazono, K. (2002). Two major Smad pathways in TGF-beta superfamily signalling. Genes Cells *7*, 1191–1204.

Muñoz-Sanjuán, I., and Brivanlou, A.H. (2002). Neural induction, the default model and embryonic stem cells. Nat. Rev. Neurosci. *3*, 271–280.

Peñuelas, S., Anido, J., Prieto-Sánchez, R.M., Folch, G., Barba, I., Cuartas, I., García-Dorado, D., Poca, M.A., Sahuquillo, J., Baselga, J., et al. (2009). TGF-beta increases glioma-initiating cell self-renewal through the induction of LIF in human glioblastoma. Cancer Cell *15*, 315–327.

Piccirillo, S.G., Reynolds, B.A., Zanetti, N., Lamorte, G., Binda, E., Broggi, G., Brem, H., Olivi, A., Dimeco, F., and Vescovi, A.L. (2006). Bone morphogenetic proteins inhibit the tumorigenic potential of human brain tumour-initiating cells. Nature *444*, 761–765.

Pramoonjago, P., Baras, A.S., and Moskaluk, C.A. (2006). Knockdown of Sox4 expression by RNAi induces apoptosis in ACC3 cells. Oncogene *25*, 5626–5639.

Sánchez-Capelo, A. (2005). Dual role for TGF-beta1 in apoptosis. Cytokine Growth Factor Rev. *16*, 15–34.

Sawyer, J.S., Anderson, B.D., Beight, D.W., Campbell, R.M., Jones, M.L., Herron, D.K., Lampe, J.W., McCowan, J.R., McMillen, W.T., Mort, N., et al. (2003). Synthesis and activity of new aryl- and heteroaryl-substituted pyrazole inhibitors of the transforming growth factor-beta type I receptor kinase domain. J. Med. Chem. *46*, 3953–3956.

Schlingensiepen, K.H., Schlingensiepen, R., Steinbrecher, A., Hau, P., Bogdahn, U., Fischer-Blass, B., and Jachimczak, P. (2006). Targeted tumor therapy with the TGF-beta2 antisense compound AP 12009. Cytokine Growth Factor Rev. *17*, 129–139.

Schmitz, M., Temme, A., Senner, V., Ebner, R., Schwind, S., Stevanovic, S., Wehner, R., Schackert, G., Schackert, H.K., Fussel, M., et al. (2007). Identification of SOX2 as a novel glioma-associated antigen and potential target for T cell-based immunotherapy. Br. J. Cancer *96*, 1293–1301.

Singh, S.K., Hawkins, C., Clarke, I.D., Squire, J.A., Bayani, J., Hide, T., Henkelman, R.M., Cusimano, M.D., and Dirks, P.B. (2004). Identification of human brain tumour initiating cells. Nature *432*, 396–401.

Surawicz, T.S., Davis, F., Freels, S., Laws, E.R., and Menck, H.R. (1998). Brain tumor survival: results from the National Cancer Data Base. J. Neurooncol. *40*, 151–160.

Takahashi, K., Tanabe, K., Ohnuki, M., Narita, M., Ichisaka, T., Tomoda, K., and Yamanaka, S. (2007). Induction of pluripotent stem cells from adult human fibroblasts by defined factors. Cell *131*, 861–872.

Takahashi, K., and Yamanaka, S. (2006). Induction of pluripotent stem cells from mouse embryonic and adult fibroblast cultures by defined factors. Cell *126*, 663–676.

Tojo, M., Hamashima, Y., Hanyu, A., Kajimoto, T., Saitoh, M., Miyazono, K., Node, M., and Imamura, T. (2005). The ALK-5 inhibitor A-83-01 inhibits Smad signaling and epithelial-to-mesenchymal transition by transforming growth factor-beta. Cancer Sci. *96*, 791–800.

Tomioka, M., Nishimoto, M., Miyagi, S., Katayanagi, T., Fukui, N., Niwa, H., Muramatsu, M., and Okuda, A. (2002). Identification of Sox-2 regulatory region which is under the control of Oct-3/4-Sox-2 complex. Nucleic Acids Res. *30*, 3202–3213.

Tso, C.L., Shintaku, P., Chen, J., Liu, Q., Liu, J., Chen, Z., Yoshimoto, K., Mischel, P.S., Cloughesy, T.F., Liau, L.M., et al. (2006). Primary glioblastomas express mesenchymal stem-like properties. Mol. Cancer Res. *4*, 607–619.

Vescovi, A.L., Galli, R., and Reynolds, B.A. (2006). Brain tumour stem cells. Nat. Rev. Cancer *6*, 425–436.

Xu, R.H., Sampsell-Barron, T.L., Gu, F., Root, S., Peck, R.M., Pan, G., Yu, J., Antosiewicz-Bourget, J., Tian, S., Stewart, R., et al. (2008). NANOG is a direct target of TGFbeta/activin-mediated SMAD signaling in human ESCs. Cell Stem Cell *3*, 196–206.

Yokota, N., Mainprize, T.G., Taylor, M.D., Kohata, T., Loreto, M., Ueda, S., Dura, W., Grajkowska, W., Kuo, J.S., and Rutka, J.T. (2004). Identification of differentially expressed and developmentally regulated genes in medulloblastoma using suppression subtraction hybridization. Oncogene *23*, 3444–3453.

J Neurooncol (2009) 93:275–278
DOI 10.1007/s11060-008-9771-6

CASE REPORT

A case of central nervous system lymphomatoid granulomatosis; characteristics of PET imaging and pathological findings

Hiroshi Nishihara · Matsuyoshi Nakasato · Hiroki Sawa · Hiromi Murakami · Daisuke Yamamoto · Kenji Moriyama · Norifumi Kato · Ikuo Hashimoto · Hajime Kamada · Shinya Tanaka

Received: 26 September 2008 / Accepted: 10 December 2008 / Published online: 23 December 2008

Abstract Lymphomatoid granulomatosis (LYG) in the central nervous system (CNS) is an uncommon lymphoproliferative disorder with low grade malignant potential. Here we report a case of CNS-LYG, in particular, its characteristics of radioisotope imaging and pathological findings. A 65-year-old man complained of visual disturbance and homonymous hemianopsia was designated. CT and MRI revealed an edematous, enhanced irregular and nodular lesion in the right occipital and parietal lobes. Although 18F-fluorodeoxyglucose (FDG)-positron emission tomography (PET) scan showed low uptake in the lesion, Methionine (MET)-PET scan indicated high uptake. Proton magnetic resonance spectroscopy (^{1}H-MRS) at 3T revealed a decrease of the peak of the *N*-acetylaspartate (NAA), suggesting a possible neoplastic lesion. The patient was diagnosed with CNS-LYG based on the surgically removed material showing perivascular infiltration of CD3-positive small T-lymphocytes with granulomatous lesions. The post-operative steroid therapy was effective and the recurrence or exacerbation has not been observed by radiological imaging until now.

Keywords Lymphomatoid granulomatosis · FDG-PET · MET-PET

H. Nishihara (✉)
Laboratory of Translational Pathology, Hokkaido University School of Medicine, N15W7, Kita-Ku, Sapporo 060-8638, Japan
e-mail: nisihara@patho2.med.hokudai.ac.jp

M. Nakasato · I. Hashimoto · H. Kamada
Department of Neurosurgery, Hokuto Hospital, Obihiro, Japan

H. Sawa · H. Murakami
Laboratory of Oncology, Hokuto Hospital, Obihiro, Japan

D. Yamamoto · K. Moriyama · N. Kato
Department of Radiology, Hokuto Hospital, Obihiro, Japan

S. Tanaka
Laboratory of Cancer Research, Department of Pathology, Hokkaido University School of Medicine, Sapporo, Japan

Introduction

Central nervous system-lymphomatoid granulomatosis (CNS-LYG), exhibiting a characteristic angiocentric infiltrate associated with abundant macrophages and small lymphocytes, is categorized into lymphoproliferative disorder with low grade malignant potential of essential T-cell phenotype except for the EBV-associated cases [1]. Neurological symptoms vary and are nonspecific; in addition, laboratory findings usually are unremarkable and thus the diagnosis of CNS-LYG usually is delayed and difficult. Radiologically, CNS-LYG shows the multiple punctate and linear enhancement on CT and MR imaging, which is characteristic of LYG since it may represent perivascular tissue and walls of small vessels [2]; however, the evaluation of CNS-LYG using radioisotope imaging, such as FDG- or MET-PET, has not been demonstrated yet. In this report, we described a case of CNS-LYG especially with radioisotope imaging in addition to pathophysiological findings.

Case report

History and examination

A 65-year-old man was admitted to Hokuto Hospital due to failure of eyesight, and designated homonymous

hemianopsia. T1- and T2-weighted magnetic resonance (MR) images showed an irregular and nodular lesion with peripheral edema in the right occipital and temporal lobes (Fig. 1a, b). FDG-PET showed a low uptake (Fig. 1c), while MET-PET indicated a high uptake in this lesion (Fig. 1d). ^{1}H-MRS exhibited an increased peak of choline and a decreased peak of the NAA (Fig. 1e), suggesting the presence of tumor lesions such as glioma or malignant lymphoma, as well as infarction. The total resection of the lesion was performed and lymphomatoid granulomatosis was diagnosed based on the histopathological examination. The steroid therapy was admitted and the recurrence or exacerbation was not seen for 10 months after operation.

Pathological findings

The brain lesions consisted of inflammatory destruction of the cerebral cortex due to mononuclear cell infiltration including small lymphoid cells without overt nuclear atypism and microglia/macrophages, which were often prominent in the perivascular areas (Fig. 2a). Immunohistochemically, the infiltrated small lymphoid cells were labeled with anti-CD3 antibody (Ab) (Fig. 2b), showing a T cell phenotype, and accompanied by CD20 positive reactive B-cells (Fig. 2c) and scattered aggregates of CD68 positive macrophages (Fig. 2d). An ISH for EBV-encoded small ribonucleic acid (RNA; EBER-1) disclosed that nuclei of the infiltrated cells were negative for EBER-1 (data not shown). These findings suggested that the lesion could be diagnosed as CNS-LYG rather than overt malignant lymphoma.

Discussion

The reported radiological appearance of CNS-LYG using CT and MRI has varied and has been nonspecific [2], while the radioisotope evaluation for CNS-LYG has not been well characterized. In this case, MR imaging revealed an irregular and nodular lesion with peripheral edema in the right occipital and temporal lobes as shown in Fig. 1; therefore, our initial diagnosis was a brain tumor such as glioma. Applications of FDG-PET for tumor imaging have proved to be highly useful for the diagnosis of primary brain tumors; however, the sensitivity of detection for low grade tumors is not crucial because of the relatively small differences in the rates of glucose utilization between a normal brain and low grade tumors [3]. In fact, low- or iso-uptake in FDG accumulation in the lesions of CNS-LYG, a possible low grade malignant lymphoproliferative disorder, was observed in our study and in a previous report [4]. On the other hand, MET-PET is the most popular amino acid (AA)-imaging modality for brain tumors, because the uptake of AA in a normal brain is low and the contrast between a tumor and a normal brain is generally better with AA scanning as compared to FDG-PET. Thus, MET-PET allows for the identification of low grade brain tumors including gliomas, even when no uptake is visible on FDG-PET [3]. Furthermore, such a discrepancy between FDG- and MET-PET study has been described in the case of low grade malignant lymphoma [5]. In this study, MET-PET exhibited a high uptake in the lesion compatible with malignant glioma (Fig. 1d), while FDG-PET described a rather low uptake lesion suggesting a necrotizing lesion

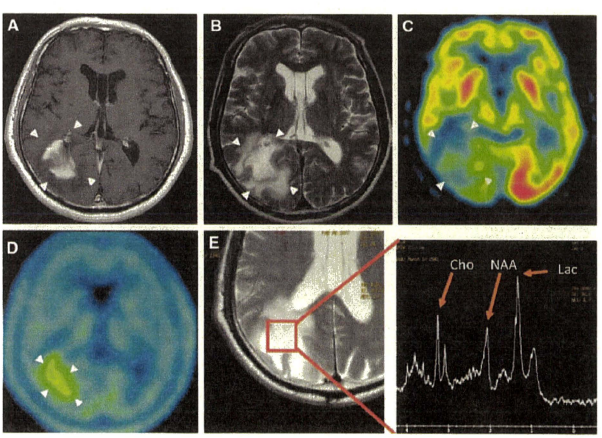

Fig. 1 T1(**a**)- and T2(**b**)-weighted MR images indicated an irregular and nodular lesion with peripheral edema in the right occipital and temporal lobes (arrowheads). FDG-PET showed a low uptake (**c**, arrowheads), and MET-PET indicated a high uptake in this lesion (**d**, arrowheads). ^{1}H-MRS exhibited an increased peak of choline (Cho) and lactate (Lac), and it showed a decreased peak of the N-acetylaspartate (NAA) (Fig. 1e, right panel)

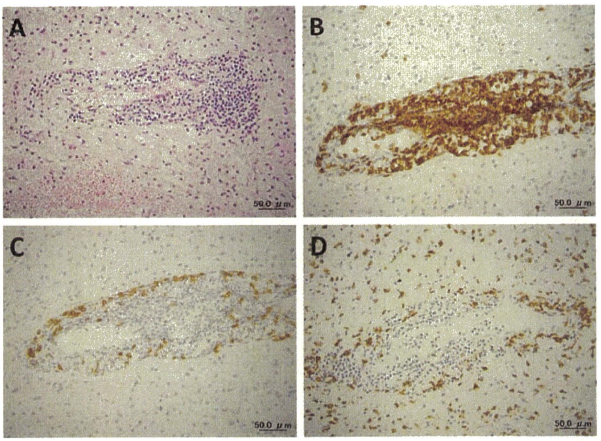

Fig. 2 Histological features of a brain biopsy specimen from the right occipital lobe. HE staining showed mononuclear cell infiltration confined to the perivascular area and inflammatory destruction of the cerebral cortex with hemorrhage and edema. Infiltrates were small lymphocytes with no overt nuclear atypism (**a**, x400). Immunihistochemically, the infiltrates were positive for anti-CD3 (**b**, x400) Abs. and CD20-positive B-cells were barely observed (**c**, x400). In particular, scattered granuloma like lesions composed of numerous CD68-positive macrophages were present (**d**, x400)

such as brain infarction (Fig. 1c). We propose that this mismatched accumulation in FDG- and MET-PET could be a characteristic radioisotope evaluation for CNS-LYG, although we should not ignore the possibility of other necrotic or inflammatory lesions. In addition, here we employed ^{1}H-MRS on this disease, and obtained the increased peak of choline suggesting the presence of a tumor and the decreased peak of the NAA indicating the loss of nervous tissue. The increased peak of lactate was also observed, suggesting the presence of necrosis. These findings are almost compatible with the histological appearance of CNS-LYG which consists of inflammatory destruction of the cerebral cortex due to small lymphoid cell infiltration accompanied by edematous granulation tissue. Our results propose that MRS could be a useful examination for the diagnosis of CNS-LYG as well as PET imagings, although this is the first report of MRS study on CNS-LYG and we should compile certain numbers of the case studies to evaluate the usefulness of MRS.

The large part of CNS-LYG is classified as lymphoproliferative disorder with low grade malignant potential of essential T-cell phenotype contrary to predominant B-cell phenotype of systemic-LYG [1]. In this case, the brain specimen was composed of perivascular infiltration of CD3-positive T-cells without overt nuclear atypism and accompanied by granulomatous lesions. Although the PCR-SSCP method to detect T-cell Receptor gene rearrangement using the paraffin-embedded specimen represented a smear polyclonal band (data not shown), based on these histological findings, we diagnosed CNS-LYG, differently from T-cell malignant lymphoma. In fact, the recurrence or exacerbation was not observed for 10 months after operation on this patient after steroid treatment, and such indolent clinical course is supporting our diagnosis of CNS-LYG.

The initial description of LYG was necrotizing inflammatory lesions [6–10]; however, the prognosis of this disease has been considered to be relatively poor with a mortality rate ranging from 65 to 90% and with progression to malignant lymphoma in 13% [11]. CNS-LYG is still a controversial lymphoproliferative disease including T-cell and B-cell phenotype, and we should not ignore the potential malignancy of CNS-LYG such as dissemination to systemic lymphoreticular system described previously [12]. The majority of cases of CNS-LYG appear to be T-cell phenotype [1] and the patients should have adequate treatments such as steroid and/or radiation therapy effective for T-cell lymphoma. On the other hand, the specific therapy for B-cell lymphoma, such as Rituximab, may be applicable for the case of B-cell phenotype associated with EB virus, although it is extremely rare among CNS-LYG [1].

Here our research results represent the characteristic results of FDG/MET-PET and MRS for CNS-LYG; however, the findings of radioisotope imagings are not specific for CNS-LYG. Thus, the histopathological evaluation is indispensable for the final diagnosis and choosing the cell-type specific treatment.

References

1. Nishihara H, Tateishi U, Itoh T, Nagashima K, Tanaka S (2007) Immunohistochemical and gene rearrangement studies of central nervous system lymphomatoid granulomatosis. Neuropathology 27:413–418. doi:10.1111/j.1440-1789.2007.00804.x
2. Tateishi U, Terae S, Ogata A, Sawamura Y, Suzuki Y, Abe S, Miyasaka K (2001) MR imaging of the brain in lymphomatoid granulomatosis. AJNR Am J Neuroradiol 22:1283–1290
3. Singhal T, Narayanan TK, Jain V, Mukherjee J, Mantil J (2008) 11C-L-methionine positron emission tomography in the clinical management of cerebral gliomas. Mol Imaging Biol 10:1–18. doi:10.1007/s11307-007-0115-2
4. Kawai N, Miyake K, Nishiyama Y, Yamamoto Y, Sasakawa Y, Haba R, Kushida Y, Tamiya T, Nagao S (2006) FDG-PET findings of the brain in lymphomatoid granulomatosis. Ann Nucl Med 20:683–687. doi:10.1007/BF02984680
5. Leskinen-Kallio S, Ruotsalainen U, Nagren K, Teras M, Joensuu H (1991) Uptake of carbon-11-methionine and fluorodeoxyglucose in non-Hodgkin's lymphoma: a PET study. J Nucl Med 32:1211–1218
6. Liebow AA, Carrington CR, Friedman PJ (1972) Lymphomatoid granulomatosis. Hum Pathol 3:457–558. doi:10.1016/S0046-8177(72)80005-4
7. Kleinschmidt-DeMasters BK, Filley CM, Bitter MA (1992) Central nervous system angiocentric, angiodestructive T-cell lymphoma (lymphomatoid granulomatosis). Surg Neurol 37:130–137. doi:10.1016/0090-3019(92)90189-T
8. Whelan HT, Moore P (1987) Central nervous system lymphomatoid granulomatosis. Pediatr Neurosci 13:113–117. doi:10.1159/000120313
9. Minars N, Kay S, Escobar MR (1975) Lymphomatoid granulomatosis of the skin. A new clinocopathologic entity. Arch Dermatol 111:493–496. doi:10.1001/archderm.111.4.493
10. Matthay RA, Bromberg SI, Putman CE (1980) Pulmonary renal syndromes—a review. Yale J Biol Med 53:497–523
11. Katzenstein AL, Carrington CB, Liebow AA (1979) Lymphomatoid granulomatosis: a clinicopathologic study of 152 cases. Cancer 43:360–373. doi:10.1002/1097-0142(197901)43:1<360::AID-CNCR2820430151>3.0.CO;2-8
12. Takiyama A, Nishihara H, Tateishi U, Kimura T, Lei W, Marukawa K, Itoh T, Hashino S, Nagashima K, Tanaka S (2008) CNS lymphomatoid granulomatosis with lymph node and bone marrow involvements. Neuropathology 28:640–644. doi:10.1111/j.1440-1789.2008.00903.x

Journal of Controlled Release 140 (2009) 306–311

Contents lists available at ScienceDirect

Journal of Controlled Release

journal homepage: www.elsevier.com/locate/jconrel

Enhanced magnetic resonance imaging of experimental pancreatic tumor *in vivo* by block copolymer-coated magnetite nanoparticles with TGF-β inhibitor

Michiaki Kumagai [a,e,1], Mitsunobu R. Kano [b,f,1], Yasuyuki Morishita [b], Motomi Ota [a], Yutaka Imai [a], Nobuhiro Nishiyama [a,e,f], Masaki Sekino [c], Shoogo Ueno [d], Kohei Miyazono [b,f], Kazunori Kataoka [a,e,f,*]

[a] Department of Materials Engineering, Graduate School of Engineering, The University of Tokyo, 7-3-1 Hongo, Bunkyo-ku, Tokyo 113-8656, Japan
[b] Department of Molecular Pathology, Graduate School of Medicine, The University of Tokyo, 7-3-1 Hongo, Bunkyo-ku Tokyo 113-0033, Japan
[c] Department of Advanced Energy, Graduate School of Frontier Sciences, The University of Tokyo, 5-1-5, Kashiwanoha, Kashiwa-shi, Chiba, 277-8561, Japan
[d] Department of Applied Quantum Physics, Graduate School of Engineering, Kyushu University, 6-10-1 Hakozaki, Higashi-ku Fukuoka 812-8581, Japan
[e] Center for Disease Biology and Integrative Medicine, School of Medicine, The University of Tokyo, 7-3-1 Hongo, Bunkyo-ku, Tokyo 113-0033, Japan
[f] Center for NanoBio Integration, The University of Tokyo, 7-3-1 Hongo, Bunkyo-ku, Tokyo 113-8656, Japan

ARTICLE INFO

Article history:
Received 13 March 2009
Accepted 5 June 2009
Available online 12 June 2009

Keyword:
Magnetic resonance imaging
Pancreatic cancer
TGF-β
Magnetite nanoparticles
Poly(ethylene glycol)

ABSTRACT

Early detection of solid tumors, particularly pancreatic cancer, is of substantial importance in clinics. Enhanced magnetic resonance imaging (MRI) with iron oxide nanoparticles is an available way to detect the cancer. The effective and selective accumulation of these nanoparticles in the tumor tissue is needed for improved imaging, and in this regard, their longevity in the blood circulation time is crucial. We developed here block copolymer-coated magnetite nanoparticles for pancreatic cancer imaging, by means of a chelation between the carboxylic acid groups in poly(ethylene glycol)–poly(aspartic acid) block copolymer (PEG–PAsp) and Fe on the surface of the iron oxide nanoparticles. These nanoparticles had considerably narrow distribution, even upon increased ionic strength or in the presence of fetal bovine serum. The PEG–PAsp-coated nanoparticles were further shown to be potent as a contrast agent for enhanced MRI for an experimental pancreatic cancer, xenografts of the human-derived BxPC3 cell line in BALB/c nude mice, with combined administration of TGF-β inhibitor. Iron staining of tumor tissue confirmed the accumulation of the nanoparticles in tumor tissue. Use of the PEG–PAsp-coated magnetite nanoparticles, combined with the TGF-β inhibitor, is of promising clinical importance for the detection of intractable solid cancers, including pancreatic cancer.

1. Introduction

Pancreatic cancer, one of the intractable solid tumors, is the fourth leading cause of cancer-related deaths in the United States and the fifth in Japan [1]. The average survival period of patients suffering from advanced pancreatic adenocarcinoma is still extremely short, only 6 months, despite recent progress in the chemotherapies [2]. Although cancer detection and treatment have been greatly improved through the development of diagnostic imaging modalities, it is still difficult to detect pancreatic cancer [3]. Consequently, the development of diagnostic systems to detect these cancers is of great importance.

Recently, superparamagnetic iron oxide (SPIO) nanoparticles composed of either magnetite (Fe_3O_4) or maghemite (g-Fe_2O_3) have been studied as contrast agents for magnetic resonance (MR) imaging [4]. Commercial application for human diagnosis based on SPIO particles is currently available. However, since cancer detection requires the systemic administration of iron oxide nanoparticles, the circulation time of the particles must be prolonged. Several studies have already reported that the behavior of magnetic nanoparticles in the bloodstream depends closely on their nanoscale morphology, including overall diameter, size distribution, or nature of the surface [5,6]. Additionally, the surface modification of iron oxide nanoparticles has proved a versatile strategy for improving their biological performance, including the reduction of immunogenicity and enhancement of targeted delivery to specific tissues [7]. However, the overall correlation between the surface modification of nanoparticles and their *in vivo* behavior remains to be further elucidated.

Various methods of stabilization for SPIO nanoparticles have been reported to date [8]. One of the most feasible approaches could be the stabilization of SPIO by coated with biocompatible polymers [9]. Suitable polymers, including poly(ethylene glycol) (PEG) and its block copolymers, are promising for the development of SPIO systems with defined surface properties. This coating of particles with PEG, or PEGylation, to avoid their uptake by the reticuloendothelial system, is under intensive investigation. We also previously reported the accumulation of β-FeOOH nanoparticles coated with PEG–poly(α,β-aspartic acid) block copolymer

* Corresponding author. Department of Materials Engineering, Graduate School of Engineering, The University of Tokyo, 7-3-1 Hongo, Bunkyo-ku, Tokyo 113-8656, Japan.
E-mail address: kataoka@bmw.t.u-tokyo.ac.jp (K. Kataoka).
[1] Equal contribution.

0168-3659/$ – see front matter © 2009 Elsevier B.V. All rights reserved.
doi:10.1016/j.jconrel.2009.06.002

(PEG–PAsp) into experimental colon adenocarcinoma, which could be applicable for tumor-selective MR imaging [10]. The multivalent bonding of PEG-based block copolymer to magnetic nanoparticles may thus help to facilitate the accumulation of these nanoparticles into some solid tumors. However, magnetic nanoparticles of any design have not yet been successful in exhibiting sufficient accumulation in intractable solid cancers, including pancreatic adenocarcinoma [1]. In addition to improving the performance of iron-based contrast agents (e.g. biocompatibility), the co-administration of adjuvant small molecules could increase the accumulation of these agents in target cancer tissue. In fact, we have recently shown that the administration of the small molecule TGF-β inhibitor (LY364947) at a low dose [11], which could minimize the potential side effects of the TGF-β inhibitor, can alter the tumor microenvironment and enhance the EPR effect in these cancers [12]. Therefore, the combined use of TGF-β inhibitor could be promising to diagnose intractable cancers with a long-circulating MRI contrast agent. Here, we demonstrated the successful MR imaging of experimental pancreatic cancer by the systemic administration of newly developed SPIO nanoparticles coated by PEG–PAsp in aid of TGF-β inhibitor.

2. Materials and methods

2.1. Reagents

β-benzyl L-aspartate and bis(trichloromethyl)carbonate (triphosgene) were purchased from Sigma-Aldrich Corporation (St. Louis, MO, USA) and Tokyo Chemical Industry Co., Ltd. (Tokyo, Japan), respectively. α-Methoxy-ω-amino-poly(ethylene glycol) (CH_3O–PEG–NH_2; $M_w = 12000$) was purchased from NOF Corporation (Tokyo, Japan). Tetrahydrofuran (THF), *n*-hexane, *N,N*-dimethylformamide (DMF), CH_2Cl_2 were doubly-distilled according to the standard procedures. The magnetite nanoparticles were supplied by Toda Kogyo Corporation (Hiroshima, Japan; average particle size of magnetite: 10 nm). Resovist® was obtained from Bayer HealthCare Co., Ltd. (Osaka, Japan). TGF-β inhibitor was purchased from EMD Chemicals Inc. (San Diego, CA, USA) (LY364947; catalog no. 616451).

2.2. Synthesis of poly(ethylene glycol)–poly(α,β-aspartic acid) block copolymer (PEG–PAsp)

PEG–PAsp was synthesized by a previously reported procedure [13]. Briefly, poly (ethylene glycol)–*b*–poly(β-benzyl L-aspartate) block copolymer (PEG–PBLA) was prepared by ring-opening polymerization of N-carboxy anhydride of β-benzyl L-aspartate (BLA-NCA) from the ω-NH_2 group of PEG ($M_w = 1.2 \times 10^4$). Molecular weight distribution of PEG–PBLA was narrow as $M_w/M_n = 1.06$, which was determined by gel permeation chromatography [columns: TSK-gel G3000HHR, G4000HHR (Tosoh, Yamaguchi, Japan); eluent: DMF containing 10 mM LiCl; flow rate: 0.8 ml/min; detector: refractive index (RI); temperature: 40 °C]. The composition of these block copolymers was determined by ^{1}H NMR from peak intensity ratios of methylene protons of PEG (OCH_2CH_2: $d = 3.7$ ppm) and phenyl protons of the β-benzyl groups of PBLA ($-CH_2C_6H_5$: $d = 7.3$ ppm). The polymerization degree of BLA in block copolymer was calculated to be 38. The benzyl groups of PEG–PBLA were then removed by alkaline hydrolysis using 0.1 N NaOH to obtain PEG–PAsp as follows:

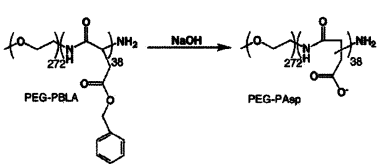

2.3. Preparation of PEG–PAsp-coated magnetite nanoparticles

PEG–PAsp-coated magnetite nanoparticles were prepared according to the previous method with slight modification [10]. Briefly, magnetite solution was quickly added to an aqueous solution of PEG–PAsp with varying feed molar ratios of aspartic acid residues to Fe ([Asp]/[Fe]) in the range of 0.01 to 1. The final concentration of magnetite was adjusted to 10 mmol/l. The mixed solutions were incubated at room temperature for 24 h to obtain magnetite nanoparticles coated with PEG–PAsp. Purification of the PEG–PAsp-coated magnetite nanoparticles was carried out by ultrafiltration (MWCO 200 000; polysulfone membrane, Toyo Roshi Co. Ltd., Tokyo, Japan).

2.4. Physicochemical characterization of the nanoparticles

The morphology and size distribution of the nanoparticles were examined by transmission electron microscopy (H-7000, Hitachi, Ltd., Tokyo, Japan) at an accelerating voltage of 75 kV. The TEM samples were prepared by mounting a drop of aqueous iron oxide nanoparticles suspension on carbon-coated 400 mesh Cu grids and allowing them to dry in air. Fourier transform infrared (FT-IR) spectra were obtained using a FT-IR spectrophotometer (FT/IR615, JASCO Corporation, Hachioji, Tokyo, Japan) with a resolution of 4 cm^{-1}. To characterize the interaction between block copolymer and magnetite nanoparticles, a small amount of nanoparticles powder was milled with KBr, and then pressed into a disc for analysis. Each spectrum was scanned 64 times to increase the signal-to-noise ratio. The Fe content in the nanoparticles was determined by ion coupled plasma-mass spectroscopy (ICP-MS, 4500, Hewlett Packard, Palo Alto, CA, USA). The amount of adsorbed block copolymer on magnetite nanoparticles was measured by thermogravimetric analysis (TGA) (EXSTAR6200 TG/DTA, Seiko Instruments Inc., Chiba, Japan) in nitrogen atmosphere with a heating rate of 10 °C/min in the temperature range of 25–1100 °C.

2.5. Light scattering and ζ-potential measurements

The size distribution of the PEG–PAsp-coated magnetite nanoparticles was examined by dynamic light scattering (DLS) DLS-7000 (Otsuka Electronics Co., Ltd., Osaka, Japan). Vertically polarized light with a wavelength of 488 nm from an Ar-ion laser (15 mW) was used as the incident beam. All measurements were conducted at 37 °C, and the data were analyzed by the cumulant method to determine the hydrodynamic diameters of the particles. The ζ-potential of PEG–PAsp-coated magnetite nanoparticles at 37 °C was measured by a Zetasizer NanoZS instrument equipped with a DTS5001 cell (Malvern Instruments Ltd., Worcestershire, UK).

2.6. Characterization of the r_2 relaxivities

The MR contrast effect of the magnetite nanoparticles was examined by measuring their proton relaxivities, r_2, of which the definition is the slope of the concentration dependence given as:

$$1/T_2 = 1/T_2(0) + r_2[\mathrm{Fe}]$$

Thus, a plot of $1/T_2$ versus concentration gives the relaxivity as the slope, where T_2 is the transversal relaxation time, $1/T_2$ is the transversal relaxation rate constant in the presence of a paramagnetic species, and $1/T_2(0)$ is the transversal relaxation rate constant in the absence of a paramagnetic species. The magnetite nanoparticles were dispersed into deionized water at concentrations of 0.5, 1.0, 1.5, 2.0, and 2.5 mM and the T_2 of these nanoparticle solutions was measured at 25 °C in water with a 0.47 T minispectrometer (Minispec, Bruker

Optics Inc., Woodlands, TX, USA) using the Carr–Purcell–Meiboom–Gill (CPMG) method [14].

2.7. In vivo MR imaging

The BxPC3 human pancreatic adenocarcinoma cell line was obtained from the American Type Culture Collection (Manassas, VA, USA). The BxPC3 cells were grown in RPMI 1640 medium supplemented with 10% FBS. BALB/c nude mice (female, 5–6 weeks of age), obtained from Charles River Laboratories Japan Inc. (Tokyo, Japan), were inoculated subcutaneously with BxPC3 cells (1×10^7 cells/mouse). After 3–4 weeks, MR imaging of the tumors was conducted with a 4.7 T scanner (INOVA200, Varian, Inc., Palo Alto, CA, USA). Twenty-four hours prior to the *in vivo* MR imaging, animals were treated with TGF-β inhibitor, 5 mg/ml in 4 μl of DMSO and diluted by 100 μl of PBS, at 1 mg/kg by intraperitoneal injection. Subsequently, the mice were injected at a dose of 0.1 mmolFe/kg, with Resovist® or PEG–PAsp-coated magnetite nanoparticles. A total of 4 conditions ($n=5$ mice each) were investigated, i.e. with or without TGF-β inhibitor for both Resovist® or PEG–PAsp-coated magnetite nanoparticles. Imaging was performed at different temporal points (e.g., preinjection, 1 h postinjection, and 2 h postinjection). For the T_2-weighted MR imaging of live mice, the following parameters were adopted: spin-echo method, point resolution = 234 × 234 μm, section thickness = 2.0 mm, TE = 60 ms, TR = 3000 ms, number of acquisitions = 5. All animals were treated in accordance with the guidelines of the Animal Ethics Committee of the University of Tokyo.

2.8. Histology

The excised samples were fixed overnight in 4% paraformaldehyde and then paraffin-embedded. Embedded samples were thin sliced at 10 μm thick and then stained using an Iron Stain Kit (Muto Pure Chemicals Co., Ltd., Tokyo, Japan), based on McFadzean's protocol [15], with nuclear post-staining by 1% Safranin O. Iron staining was observed using an AX80 microscope (Olympus Corporation, Tokyo, Japan). The photographs were further quantified using Adobe Photoshop software (Adobe Systems Incorporated, San Jose, CA, USA), ImageJ software (National Institute of Health, MD, USA), and Microsoft Excel software (Microsoft Corporation, Redmond, WA, USA).

3. Results and discussion

3.1. The physicochemical properties of the PEG–PAsp-coated magnetite nanoparticle: diameter and surface polymer density

For solid tumor diagnosis, it is important to develop well-designed magnetite nanoparticles. The key physicochemical properties of magnetite nanoparticles are size, surface polymer density, and surface charge, since these characteristics can affect accumulation of magnetite nanoparticles to solid tumor. The PEG–PAsp-coated magnetite nanoparticles were prepared by mixing solutions of magnetite nanoparticles and PEG–PAsp with various molar ratios of the Asp residues to Fe (Asp/Fe); Asp/Fe ranged from 0.01 to 0.5, where [Fe] = 10 mmol/l. As seen in Fig. 1, the transmission electron microscopy (TEM) image with 75 kV accelerating voltage of nanoparticles mounted on carbon grid from aqueous solution revealed that PEG–PAsp-coated magnetite nanoparticles take a cubic shape with a mean particle diameter of approximately 10 nm. The PEG–PAsp coating was observed as a layer with a thickness of approximately 5 nm, surrounding the magnetite nanoparticles. It was also observed in the TEM image that these PEG–PAsp-coated nanoparticles form clusters with a size range of 100 nm.

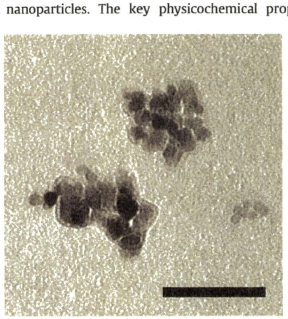

Fig. 1. TEM image of the PEG–PAsp-coated magnetite nanoparticles. Bar: 100 nm.

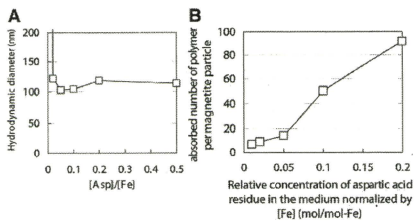

Fig. 2. Physicochemical properties of the PEG–PAsp-coated magnetite nanoparticles. (A) Hydrodynamic diameter vs. relative concentration of aspartic acid residue in the medium normalized by [Fe] (mol/mol-Fe) (=[Asp]/[Fe]), and (B) Change in the adsorbed density of PEG–PAsp on the magnetite surface estimated from TGA analysis with a bulk concentration of PEG–PAsp. Temperature = 37 °C; medium: distilled water.

The hydrodynamic diameter of these nanoparticles in aqueous medium was then measured with DLS and shown to be in the range of 100 to 120 nm with unimodal distribution, for Asp/Fe ratios ranging from 0.02–0.5. This DLS data is consistent with the cluster formation of nanoparticles indicated from TEM images. However, with a lowered Asp/Fe ratio as 0.01, the hydrodynamic diameter increased significantly (Fig. 2A). This result indicates that there is a critical surface concentration of PEG to effectively prevent the PEG–PAsp-coated magnetite nanoparticles from the agglomeration. The purified nanoparticles were stable in distilled water as 100 nm-scaled cluster at room temperature as well as at 37 °C, maintaining the initial photon count and distribution in DLS analysis for at least one month, even after the ultrafiltration to remove free PEG–PAsp possibly remained in the reactant.

The density of the PEG–PAsp block copolymer on the magnetite particle surface was estimated by TGA. Here, nanoparticles were heated in the nitrogen atmosphere to selectively vaporize the polymer fraction. Eventually, the amount of absorbed polymer on the surface of the nanoparticles was measured from the weight change by heating. The polymer density was then calculated from the TGA measurement for all the nanoparticles, assuming the cubic morphology as evidenced by microscopy and a density of 5.05 g/cm^3 for magnetite. As seen in Fig. 2B, the number of polymer strands on the nanoparticle surface was as high as 100. This data suggests that the PEG density on the magnetite nanoparticles is a little lower than that of PEGylated gold nanoparticles prepared through the surface tethering of PEG-SH [16].

3.2. The mechanism of PEG–PAsp adsorption on the magnetite nanoparticles

To confirm the formation of PEG–PAsp coating on the magnetite nanoparticles, the ζ-potential of bare and PEG–PAsp-coated magnetite nanoparticles was measured in 10 mM MOPS buffer as a function of

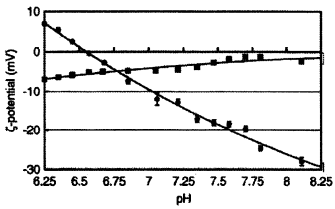

Fig. 3. Change in the ζ-potential with pH for bare (●) and PEG–PAsp-coated (■) magnetite nanoparticles. Temperature = 37 °C; medium: 10 mM MOPS buffer.

pH (Fig. 3). The isoelectric point (IEP) of the bare magnetite nanoparticles was estimated as approximately 6.6, which is consistent with the reported IEP value of iron oxide [17]. In a lower pH (below the IEP), the magnetite nanoparticle surface was protonated to result in a positive ζ-potential. Thus, in this pH range, electrostatic attraction between positively-charged magnetite nanoparticles and negatively charged PEG–PAsp is expected to occur, allowing the PEG–PAsp adsorption to the nanoparticle surface. Alternatively, the bare magnetite nanoparticles possess negative ζ-potential at physiological pH 7.4, whereas the ζ-potential shifted to the neutral value for PEG–PAsp modified nanoparticles in 10 mM MOPS buffer (pH 7.4), being consistent with the formation of a PEG shell layer. Also, these data suggest that there should be an adsorption mechanism other than simple electrostatic interaction, because magnetite has a negative ζ-potential value at pH 7.4 to induce electrostatic repulsive force against negatively charged carboxylates in PEG–PAsp. The adsorption mechanism under physiological pH was suggested to be the monodentate chelation (I) (Fig. 4) from the result of Fourier transform infrared spectroscopy [18], as explained in detail in Supplemental Text with Supplemental Fig. 1 and Supplemental Table 1.

3.3. Comparison study of the physicochemical characteristics of the PEG–PAsp- and dextran-coated magnetite nanoparticles

The MRI detection limit was compared between the PEG–PAsp- and dextran-coated magnetite nanoparticles in the field of 0.47 T at 25 °C from the relaxivity r_2, exhibiting the sensitivity of the T_2 MRI contrast agent. The dextran-coated magnetite used in this study was the one already in clinical use, Resovist®. Eventually, the relaxivity r_2 of the PEG–PAsp nanoparticle was calculated to be 138 $mM^{-1}\,s^{-1}$, the value similar to Resovist® [19].

The hydrodynamic diameter observed between the PEG–PAsp-coated and dextran-coated magnetite nanoparticles differed significantly in an NaCl-concentration-dependent manner (Fig. 5A). Although the hydrodynamic diameter of the PEG–PAsp-coated magnetite nanoparticles did not change significantly up to 3 M NaCl, indicating the appreciable stability of the PEG–PAsp-coating, that of Resovist® significantly increased even at NaCl = 0.15 M, and reached more than 1 μm at NaCl = 0.5 M, due to the drastic aggregation. Note that the PEG–PAsp-coated nanoparticles did not show any change in

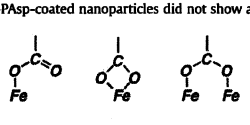

Fig. 4. Modes of carboxylate-metal complexation: monodentate (I), bidentate chelating (II), and bidentate bridging (III).

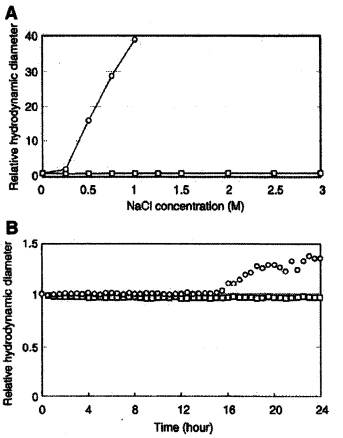

Fig. 5. NaCl concentration (A) and time (B) dependencies of the relative hydrodynamic diameter of magnetite nanoparticles, □: PEG–PAsp-coated nanoparticles, ○: dextran-coated nanoparticles (Resovist®). Fe concentration = 2 mmol/l; temperature = 37 °C; medium 10 mM Tris–HCl buffered saline (pH 7.4). 10% fetal bovine serum was contained in (B).

their size even after one month storage in 10 mM Tris–HCl buffered saline (pH 7.4, 37 °C) (data not shown).

The colloidal stability of the PEG–PAsp-coated magnetite nanoparticles in physiological conditions was also examined. We incubated them in 10 mM Tris–HCl buffered saline (pH 7.4) containing 10% fetal bovine serum at 37 °C for 24 h and measured the change of the hydrodynamic diameter (Fig. 5B). The size of the PEG–PAsp-coated magnetite nanoparticles did not obviously change during the 24-hour storage time. On the other hand, the size of Resovist® increased by the formation of aggregates after 16 h of storage time.

The stability of the PEG–PAsp-coated nanoparticles may come from the multivalent bonding between flanking carboxylic groups and the magnetite surface, as suggested by FT-IR study. These findings are consistent with a report showing that PEG-oligo(aspartic acid) block copolymer-coated iron oxide nanoparticles were stable at pH 2–11 and in 1 M NaCl, where the repeating number of aspartic acid units was 3 or more [20]. In contrast, instability of Resovist® against salt addition may be due to weak interaction between magnetite and hydroxyl groups of dextran [21].

3.4. MR imaging of experimental pancreatic cancer in vivo

The MR imaging of tumor tissue *in vivo* was then conducted by comparing PEG–PAsp- and dextran-coated magnetite nanoparticles, Resovist®. Resovist® has already been approved for clinical use as a liver-specific MRI contrast agent, due to accumulation into the reticuloendothelial system (RES) of the normal liver. Most malignant liver tumors do not contain RES cells and therefore are contrasted positive by Resovist®. A xenografted BxPC3 human pancreatic adenocarcinoma cell line in nude mice, characterized histologically by fibrosis and hypovascularity, was used as a model of intractable cancer. Recently, we reported that the administration of TGF-β inhibitor to tumor model mice significantly enhanced the intratumoral accumulation of nanoparticles encapsulating anticancer drugs [11]. Thus, we tested the effect of the i.p. administration of TGF-β

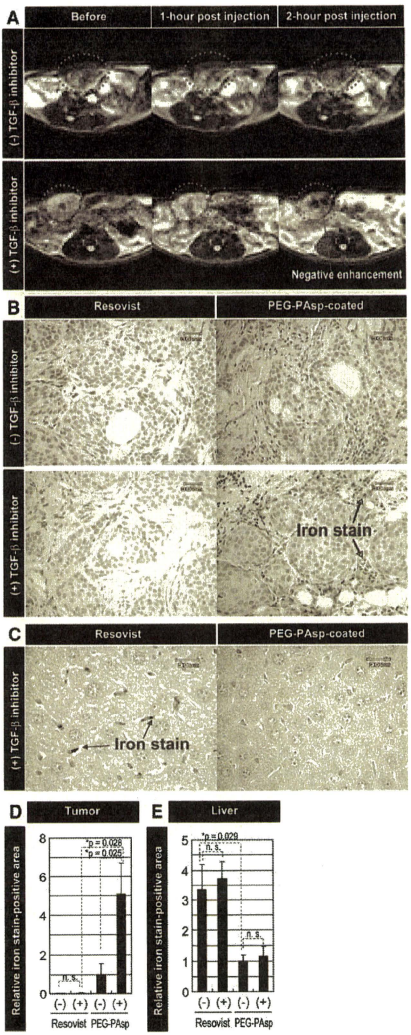

Fig. 6. MR imaging of experimental pancreatic cancer *in vivo* and the distribution of the nanoparticles in cancer and liver tissues. (A) T_2-weighted images of tumor-implanted mice (tumor sites are circled by red dotted line) at different temporal points after injection of PEG–PAsp-coated magnetite nanoparticles and TGF-β inhibitor. All images were obtained in a field strength of 4.7 T. (B) Histological sections of BxPC3 xenograft stained with Prussian blue. The distribution of Resovist® and PEG–PAsp-coated magnetite nanoparticles, at 5.5 mg/kg with and without TGF-β inhibitor at 1 mg/kg, were examined 24 h after the administration. (C) Histological sections of liver stained with Prussian blue. The distribution of Resovist® and PEG–PAsp-coated magnetite nanoparticles, at 5.5 mg/kg with TGF-β inhibitor at 1 mg/kg, was examined 24 h after the administration. (D and E) Areas of iron staining in the tumor and liver were quantified. PEG–PAsp, PEG–PAsp coated magnetite nanoparticles with (+) and without (−) inhibitor. Error bars in the graphs represent standard errors of the mean ($n = 6$), and P values were calculated by two-tailed Student's t test. n.s.: not significant.